SANDIA REPORT

SAND2004-4954
Unlimited Release
Printed October 2004

Phase Transformation of Poled "Chem-prep" PZT 95/5-2Nb Ceramic Under Quasi-static Loading Conditions

Moo Y. Lee, Stephen T. Montgomery, and John H. Hofer

Prepared by
Sandia National Laboratories
Albuquerque, New Mexico 87185

Sandia is a multiprogram laboratory operated by Sandia Corporation,
a Lockheed Martin Company, for the United States Department of Energy's
National Nuclear Security Administration under Contract DE-AC04-94AL85000.

Issued by Sandia National Laboratories, operated for the United States Department of Energy by Sandia Corporation.

Available to DOE and DOE contractors from
U.S. Department of Energy
Office of Scientific and Technical Information
P.O. Box 62
Oak Ridge, TN 37831

Telephone: (865) 576-8401
Facsimile: (865) 576-5728
E-Mail: reports@adonis.osti.gov
Online ordering: http://www.doe.gov/bridge

Available to the public from
U.S. Department of Commerce
National Technical Information Service
5285 Port Royal Rd.
Springfield, VA 22161

Telephone: (800) 553-6847
Facsimile: (703) 605-6900
E-Mail: orders@ntis.fedworld.gov
Online order: http://www.ntis.gov/help/ordermethods.asp?loc=7-4-0#online

SAND 2004-4954
Unlimited Release
Printed October 2004

Phase Transformation of Poled "Chem-prep" PZT 95/5-2Nb Ceramic Under Quasi-static Loading Conditions

Moo Y. Lee
Geomechanics Department

Stephen T. Montgomery
Neutron Generator Department

John H. Hofer
Geomechanics Department

Sandia National Laboratories
P.O. Box 5800
Albuquerque, NM 87185-0751

ABSTRACT

Specimens of poled "chem-prep" PNZT ceramic from batch HF803 were tested under hydrostatic, uniaxial, and constant stress difference loading conditions at three temperatures of −55, 25, and 75°C and pressures up to 500 MPa. The objective of this experimental study was to obtain the electro-mechanical properties of the ceramic and the criteria of FE (Ferroelectric) to AFE (Antiferroelectric) phase transformations so that grain-scale modeling efforts can develop and test models and codes using realistic parameters. The poled ceramic undergoes anisotropic deformation during the transition from a FE to an AFE structure. The lateral strain measured parallel to the poling direction was typically 35 % greater than the strain measured perpendicular to the poling direction. The rates of increase in the phase transformation pressures per temperature changes were practically identical for both unpoled and poled PNZT HF803 specimens. We observed that the retarding effect of temperature on the kinetics of phase transformation appears to be analogous to the effect of shear stress. We also observed that the FE-to-AFE phase transformation occurs in poled ceramic when the normal compressive stress, acting perpendicular to a crystallographic plane about the polar axis, equals the hydrostatic pressure at which the transformation otherwise takes place.

ACKNOWLEDGEMENTS

The authors would like to acknowledge Thomas Pfeifle for the critical review of this report. The authors also thank Jeffrey Keck for overseeing fabrication of the PNZT specimens. The managerial support received from Jaime L. Moya, Justine E. Johannes, and Laurence S. Costin is also gratefully appreciated.

Table of Contents

Figures

Tables

1. Introduction

Niobium-doped lead-zirconate-titanate ceramic (PZT 95/5-2Nb, or simply "PNZT") exhibits a transformation from the ferroelectric (FE) phase to the antiferroelectric (AFE) phase in response to compressive stress (Fritz and Keck, 1978). This transformation is key to releasing bound charge from ferroelectric ceramic material under shock-wave loading to produce pulsed currents and voltages (Lysne and Percival, 1975; Bauer *et al.*, 1976). An understanding of the electromechanical response and phase transformation of PNZT during complex stress loading must be understood to effectively design and model shock-wave activated ferroelectric power sources.

A previous investigation of the pressure-induced FE-to-AFE phase transformation was limited to the unpoled "chem-prep" ceramic from lot HF803 and the mechanical behavior of the PNZT HF803 ceramic in conjunction with the polymorphic phase transformation has been reported as functions of mean stress, stress difference, and temperature (Lee *et al.*, 2003). We found that the general mechanical and phase transition behaviors of the unpoled ceramic under different loading paths were consistent with previous observations on "mixed-oxide" PNZT ceramic. However, a comparison of properties of bulk modulus obtained from the hydrostatic loading indicates that material from HF803 appears significantly stiffer than "mixed-oxide" material from HF453. The phase transformation from FE to AFE occurs in unpoled ceramic with an abrupt increase in volumetric strain of about 0.7 % when the maximum compressive stress, regardless of loading paths, equals the hydrostatic pressure at which the transformation otherwise takes place. The volumetric transformation strains observed at room temperature for HF453 were roughly 0.9 %. The smaller value of transformation strain observed for HF803 indicates the possible presence of some material in the AFE phase. The stress-volumetric strain relationship of the ceramic undergoing a phase transformation was analyzed quantitatively using a linear regression analysis. The pressure (P_{T1}^{H}) required for the onset of phase transformation as a function of temperature was best represented by a straight line, P_{T1}^{H} (MPa) = 227 + 0.76 T (°C). We also confirmed that increasing shear stress lowers the mean stress and the volumetric strain required to trigger phase transformation. At the low temperature bound (-55°C), the phase transformation was permanent and irreversible. In contrast, at the high temperature bound (75°C), the phase transformation was completely reversible as the stress-caused phase transformation was removed.

However, to date, there has been no systematic characterization of the electro-mechanical properties and phase relationships for the poled "chem-prep" ceramic even within the limited temperature and pressure range over which some ferroelectric power supplies must function reliably. The major objective of this experimental study is to provide the grain-scale models (Montgomery *et al.*, 2001 and 2004) and codes (Brannon *et al.*, 2001) with realistic electro-mechanical parameters and the phase transformation criterion for a poled "chem-prep" ceramic.

The "chem-prep" PNZT HF803 specimens were produced based on the chemical preparation process for the synthesis of PNZT powder (U.S. Patent No. 5,908,802 by Voigt

et al., 1999). The calcinated TSP38 powder was mixed with 0.9 weight % of Lucite poreformer. The average density of PNZT HF803 was 7.36 g/cm^3. The average depoling pressure was approximately 303 (±2) MPa and fell in the upper range of the depoling pressure. The average charge release was 31.9 (±0.2) μC/cm^2 (Yang, 2003).

Table 1 shows the list of mechanical tests conducted for the poled "chem-prep" PNZT-HF803 specimens. Four hydrostatic compression (HC) tests were conducted across the FE-AFE boundary at three different temperatures (-55, 25, and 75°C) to examine the temperature influence on the phase transformation of the poled ceramic. Three uniaxial compression (UC) tests were conducted at -55, 25 and 75°C. These tests were conducted to observe the superposed strains from dipole switching (Fritz and Keck, 1978; Fritz, 1979) interacting with transformation strains. A series of constant-stress-difference (CSD) tests were conducted at four stress differences (50, 100, 150, and 300 MPa) and at three different temperatures (-55, 25, and 75°C) to investigate the effect of shear stress to the initiation of FE-to-AFE phase transformation. The result of the CSD tests was used to investigate the criteria of phase transformation in "chem-prep" PNZT HF803.

Table 1. List of mechanical tests conducted for poled "chem-prep" PNZT-HF803 specimens.

Specimen no.	Test type	T (°C)	σ_1- σ_3 (MPa)	Length (mm)	Width (mm)	Height (mm)	Weight (g)	Density (g/cm^3)	Note
PNZT-P01	HC	75	0	25.40	10.80	10.80	21.67	7.32	
PNZT-P02	UC	25	σ_1	25.48	10.82	10.80	21.76	7.31	
PNZT-P03	UC	25	σ_1	25.40	10.80	10.82	21.72	7.32	
PNZT-P04	NA								1
PNZT-P05	CSD	75	150	25.38	10.82	10.82	21.74	7.32	
PNZT-P06	NA								2
PNZT-P07	HC	25	0	25.43	10.82	10.81	21.82	7.34	
PNZT-P08	CSD	-55	300	25.43	10.81	10.81	21.77	7.33	
PNZT-P09	HC	25	0	25.43	10.80	10.80	21.75	7.34	*
PNZT-P10	NA								1
PNZT-P11	HC	-55	0	25.43	10.80	10.80	21.72	7.33	
PNZT-P12	UC	-55	σ_1	25.43	10.82	10.80	21.77	7.33	
PNZT-P13	NA								3
PNZT-P14	NA								4
PNZT-P15	NA								5
PNZT-P16	CSD	-55	50	25.43	10.80	10.80	21.74	7.34	
PNZT-P17	CSD	75	100	25.43	10.80	10.82	21.72	7.31	
PNZT-P18	NA								6
PNZT-P19	CSD	25	100	25.40	10.82	10.82	21.72	7.30	
PNZT-P20	NA								2
PNZT-P21	UC	75	σ_1	25.43	10.82	10.81	21.83	7.34	*
PNZT-P22	CSD	75	50	25.40	10.82	10.80	21.75	7.33	
PNZT-P23	CSD	-55	100	25.43	10.82	10.82	21.77	7.31	
PNZT-P24	CSD	25	150	25.48	10.80	10.80	21.71	7.31	

Note: UC-Uniaxial Compression;
CSD-Constant Stress Difference;
HC-Hydrostatic Compression
NA-Not Available
σ_1-major principal stress; σ_3-minor principal stress
1- internal load cell failure;
2- data acquisition system failure;
3- intensifier leaked;
4- strain gage failure;
5- sample damaged during preparation;
6- maximum load reached before failure of the specimen
* - Lateral strains were measured both parallel and normal to the poling direction.

2. Sample Preparation and Characterization

2.1 Sample preparation

Unpoled PNZT slugs, fabricated from the "chem-prep" and sintering processes, were machined to rectangular parallelepipeds. The specimens have nominal dimensions of 10.8 × 10.8 × 25.4 mm. The dimensions fall within the range of a nominal length-to-diameter ratio of 2 to 2.5 accomplishing which assures uniform stress and strain measured in the middle of the of the sample. The ends of the specimen were ground flat within 0.003-mm tolerance. Electrode silver paste (Dupont 7095) was applied to two opposing rectangular faces of the unpoled specimens and was fired at 600°C for about 20 minutes. The electroded specimens were then "hot-poled" at 105°C under the electric bias of 20KV (Zeuch *et al.*, 1995; Yang *et al.*, 2003) corresponding to an electric field of 2KV/mm. The "hot-poled" specimens were visually inspected for significant flaws and general straightness of the surfaces. The physical dimensions of each poled specimen are listed in Table 1 with assigned test types and test conditions.

A typical instrumented specimen is shown in Figure 1. Two pairs of orthogonal sets of axial and lateral strain gages were glued on opposite sides of the specimen at mid-height of the specimen. The axial and lateral gages were oriented to be parallel and perpendicular to the long axis of the specimen, respectively. In all specimens except two (PNZT-P09 and -P22), the lateral strain gages were glued only on the unelectroded faces of the specimen, providing a measurement of the lateral strain parallel with the poling direction. In those two other specimens, additional strain gages were mounted on the electroded faces of the specimen, enabling measurements of lateral strain normal ($\varepsilon_{\text{l-normal to poling}}$) to as well as parallel with ($\varepsilon_{\text{l-parallel to poling}}$) the poling direction.

A strain-gaged specimen was placed between upper and lower silicon carbide (SiC-N) end-caps. The specimen assembly was then coated with an approximately 1-mm-thick impervious polyurethane membrane. The flexible membrane allowed the confining pressure to be applied uniformly to the surfaces of the specimen and at the same time prevented the confining fluid from infiltrating into the specimen. To maintain uniform thickness of the membrane as it cured, the specimen assembly was rotated in a lathe with the centerline of the long axis of the assembly oriented parallel with axis of rotation of the lathe.

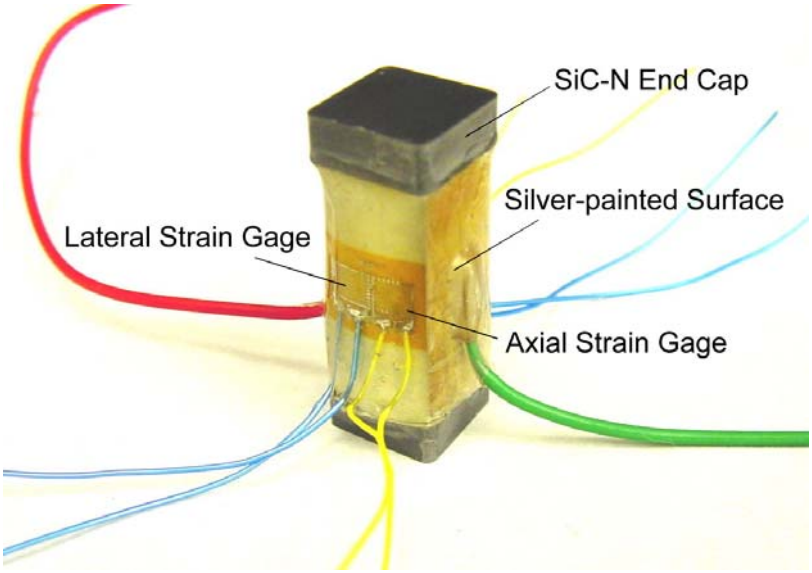

Figure 1. A typical poled "chem-prep" PNZT specimen instrumented with two pairs of axial and lateral strain gages. The specimen is placed between two silicon carbide (SiC-N) end-caps and the assembly is coated with a polyurethane membrane to prevent the confining fluid from infiltrating into the specimen.

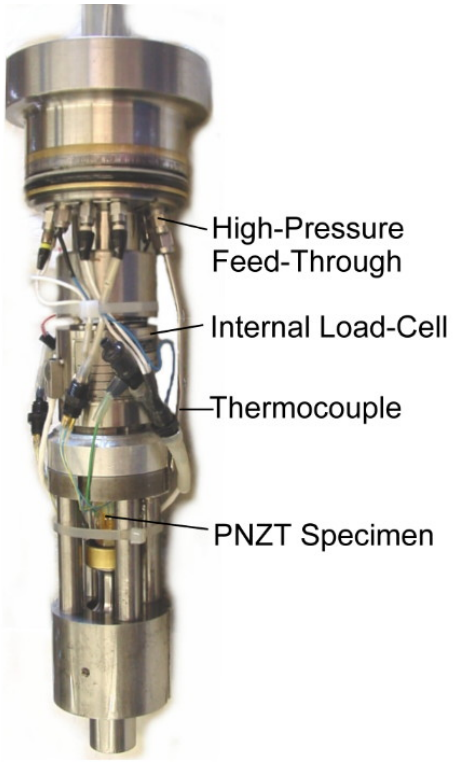

Figure 2. A PNZT specimen assembly instrumented with an internal load cell and a thermocouple.

2.2 Experimental set-up and procedure

The poled "chem-prep" PNZT HF803 specimens were tested in the High-Pressure Low-Temperature (HPLT) pressure vessel (Zeuch *et al.*, 1999d) used to characterize the electro-mechanical properties of the unpoled "chem-prep" PNZT HF803 ceramic (Lee *et al.*, 2003). The pressure vessel was made out of HP9-4-20 alloy steel. To achieve the lower temperature required for some tests, the pressure vessel was cooled externally by circulating liquid nitrogen through conduits mounted to the outside of the vessel. Elevated temperatures were achieved using an internal coil heater that surrounded the specimen. The range of operating temperatures (–65 to 150°C) and the maximum allowable pressure (500 MPa) under normal test conditions satisfied the requirements of the test matrix shown in Table 1. Figure 2 shows the specimen assembly with an internal load cell and a thermocouple. Internal data consist of axial and lateral strains, temperature, discharge voltage, and the axial load on the specimen. The data were transmitted from the internal transducers via electrical leads connected to twelve high-pressure coaxial feed-throughs. The discharge voltage that occurred during the phase transformation was measured using the circuitry shown in Figure 3 (Zeuch et. al, 1995). The charge release was drained to a capacitor where the stored voltage was measured. Confining pressure was measured using a pressure transducer mounted in the hydraulic line used to pressurize the hydraulic fluid in the vessel.

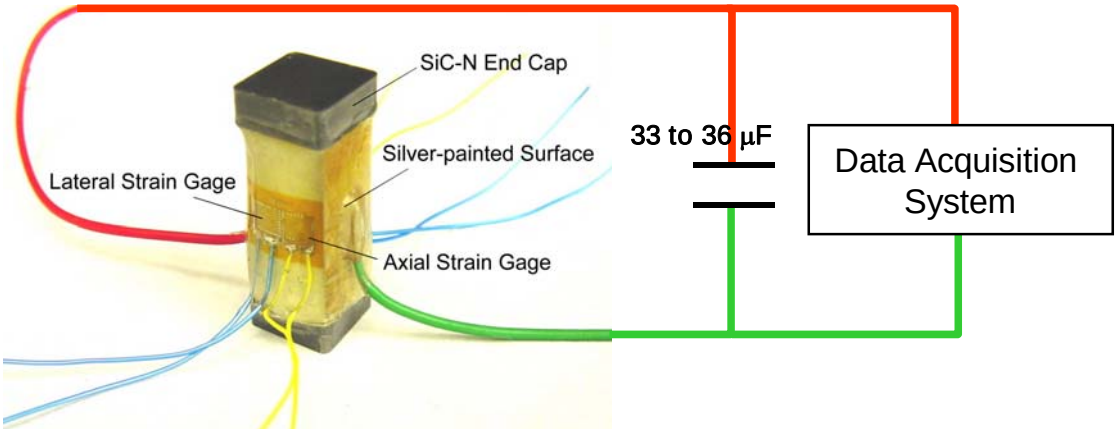

Figure 3. Measurement of charge release using a capacitor for a poled PNZT specimen.

Three different loading paths were used to characterize the phase transformation in the poled ceramic: hydrostatic compression (HC), uniaxial compression (UC), and constant stress difference (CSD). Figure 4 shows the appropriate loading path for each testing condition in terms of the maximum (σ_1) and the minimum (σ_3) principal stresses, respectively, where compression is signed positive. For the HC loading condition, the specimen was subjected to the same but simultaneously increasing principal stresses $\sigma_1=\sigma_2=\sigma_3=P$. The dashed line denoted HC in Figure 4 shows the stress path for the hydrostatic compression test. For the UC loading condition, the axial stress was applied along the long axis of the specimen without a confining pressure ($\sigma_2 = \sigma_3 = P = 0$) until the specimen failed. The loading history of the uniaxial compression (UC) test is shown as the

thick vertical line denoted UC in Figure 4. For the CSD loading condition, the specimen was initially loaded hydrostatically to a target mean stress. Following this hydrostatic loading, a stress difference (σ_1-σ_3=σ_d) was applied by independently increasing the axial stress (or σ_1) while holding the confining pressure (σ_3) constant. Finally, the axial stress and confining pressure were increased at the same rate, which maintained a constant stress difference or shear stress but resulted in increasing mean stress. The CSD load path is denoted by CSD in Figure 4.

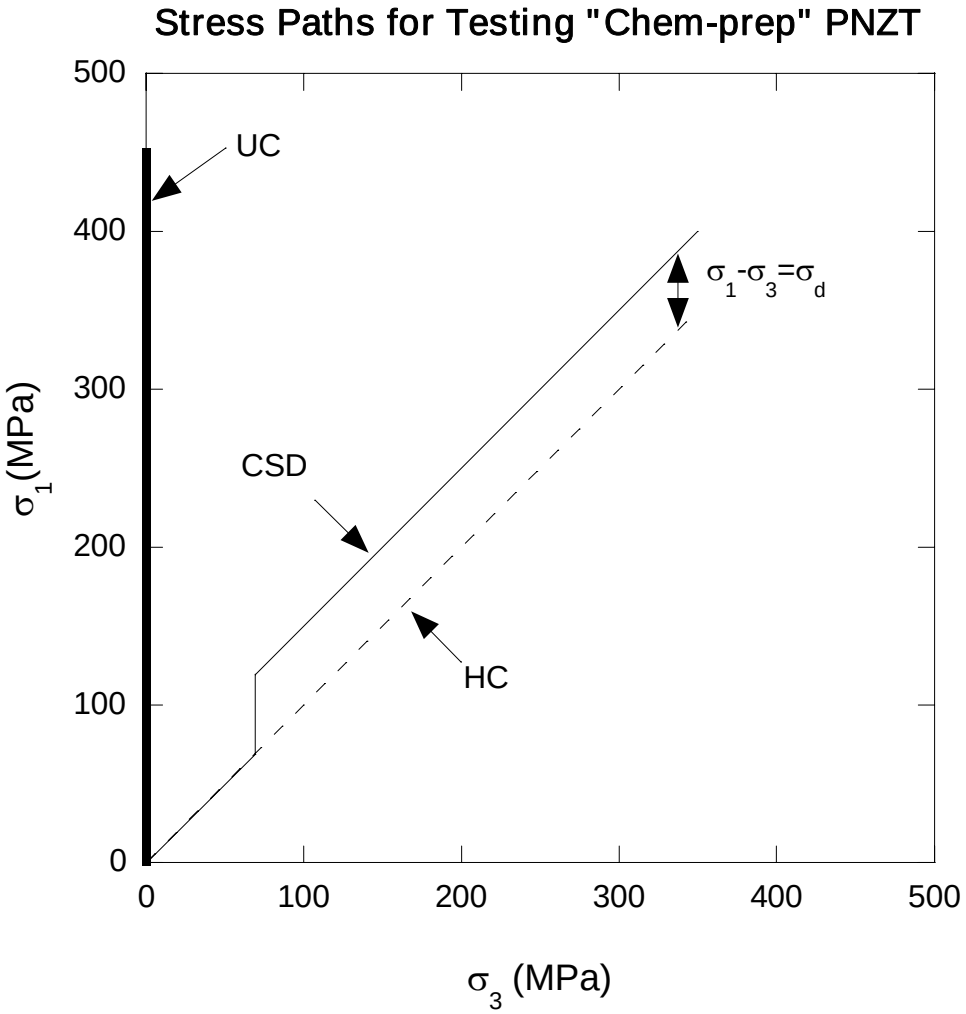

Figure 4. Three quasi-static loading paths, designed for characterization of the electro-mechanical responses of the poled "chem-prep" PNZT, are shown in the principal stress domain (UC for Uniaxial Compression, HC for Hydrostatic Compression, and CSD for Constant Stress Difference). The stress difference, σ_1-σ_3, is shown as σ_d.

3. Experimenatal characterization of poled "chem-prep" PNZT HF803

3.1 Hydrostatic compression test

FE-to-AFE phase transformation of "chem-prep" PNZT HF803 was studied under compressive hydrostatic loading conditions at temperatures of -55, 25, and 75°C, and pressures up to 500 MPa. A total of four specimens were tested and the test records of Pressure vs. Strain (axial, lateral, and volumetric) and Discharge Voltage vs. Pressure plots are shown in Appendix A.

After the specimen was placed in the HPLT vessel, the hydrostatic pressure ($\sigma_1=\sigma_2=\sigma_3=P$) was applied at a constant rate of 0.7 MPa/s. Figure 5 shows strain histories under increasing hydrostatic stress for PNZT-P09, a typical poled ceramic test specimen. The axial strains (ε_a) measured by the pair of axial strain gages were similar so only the average value of the strains is presented in this plot. Also shown are the average values of the lateral strains measured both parallel to poling ($\varepsilon_{l\text{-parallel to poling}}$) and normal to poling ($\varepsilon_{l\text{-normal to poling}}$). The individual strain gage data and the calculated volumetric strain ($\varepsilon_v = \varepsilon_a + \varepsilon_{l\text{-parallel to poling}} + \varepsilon_{l\text{-normal to poling}}$) are presented as functions of pressure in Figure 6. Similar to the unpoled PNZT HF803, the poled ceramic indicated a transition from a ferroelectric rhombohedral perovskite structure (F_{R1} or FE) to an antiferroelectric orthorhombic (A_o or AFE) structure by a sudden increase in all strains denoted by the vertical lines in Figure 5 and the horizontal lines in Figure 6. However, unlike the unpoled PNZT HF803, the poled ceramic showed an anisotropic strain behavior in the AFE phase. The lateral strain ($\varepsilon_{l\text{-parallel to poling}}$) parallel with the poling direction was greater than the lateral strain ($\varepsilon_{l\text{-normal to poling}}$) perpendicular to the poling direction by about 35 % (see Figures 5 and 6). This distinctive and repeatable anisotropic strain behaviors are caused by a preferred crystallographic orientation and locked-in, intra- and intergranular strains created by poling (Zeuch *et al.*, 1999a). The degree of anisotropy of the HF803 ceramic in lateral strains was approximately same as the results from the earlier tests on different batches of PNZT (Zeuch *et al.*, 1995 for HF424 and Lee, 2004 for HF1035).

As shown in Table 1 and in Figure 7 for PNZT-P07, the lateral strains perpendicular to the poling direction were not measured in most of the tests. For these cases, the volumetric strain, ε_v, had to be estimated from the axial strain and the available lateral strain data.

$$\begin{aligned}
&\varepsilon_v = \varepsilon_a + \varepsilon_{l\text{-parallel to poling}} + \varepsilon_{l\text{-normal to poling}} \\
&\varepsilon_{v\text{-estimated}} = \varepsilon_a + 2\varepsilon_{l\text{-parallel to poling}} \\
&\varepsilon_{l\text{-parallel to poling}} = 1.35\ \varepsilon_{l\text{-normal to poling}} \\
&\varepsilon_{v\text{-corrected}} = \varepsilon_a + 1.74\ \varepsilon_{l\text{-parallel to poling}}
\end{aligned} \qquad (1)$$

According to equation (1), uncorrected $\varepsilon_{v\text{-estimated}}$ in our plots overestimates ε_v by about 35% of $\varepsilon_{l\text{-normal to poling}}$. For later calculations of the material properties of the ceramic, we used

the corrected volumetric strain ($\varepsilon_{v\text{-corrected}}$). With or without measurements of $\varepsilon_{l\text{-normal to poling}}$, the depoling pressures can be easily identified as the pressure level corresponding to a sudden increase in strains. The anisotropy in lateral strains observed in the strain history plot was also readily identifiable from the Pressure-Strain plot.

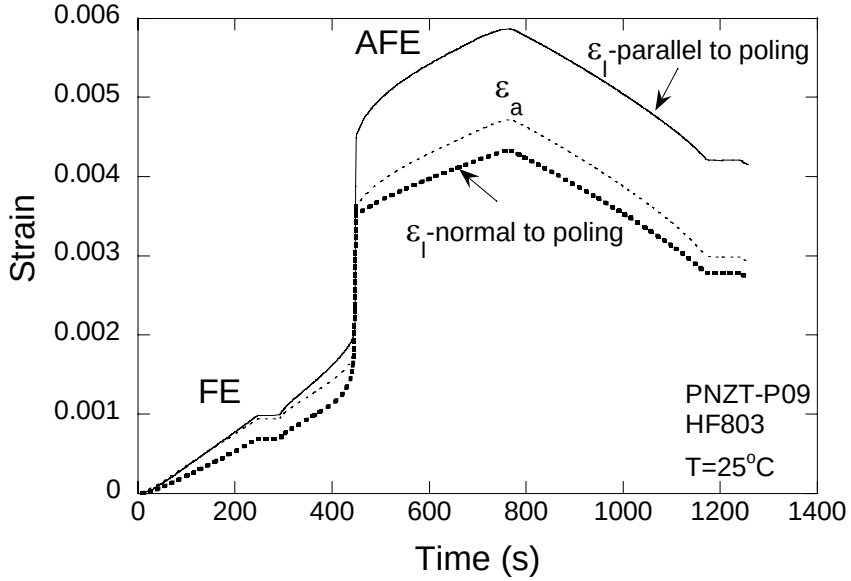

Figure 5. Phase transition and strain histories in the poled "chem-prep" PNZT-P09 specimen (ε_a – axial strain; $\varepsilon_{l\text{-parallel to poling}}$ – lateral strain parallel to poling direction, and $\varepsilon_{l\text{-normal to poling}}$ – lateral strain perpendicular to poling direction).

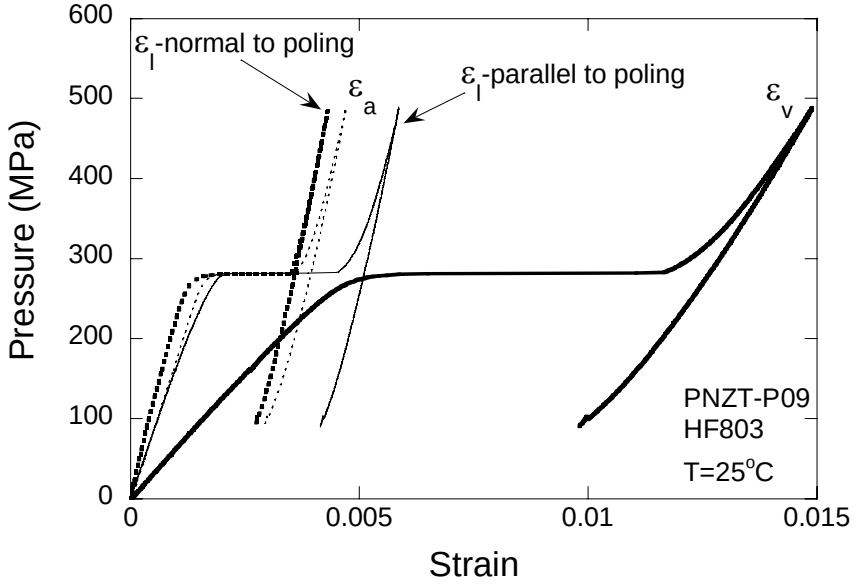

Figure 6. Phase transformation in the poled "chem-prep" PNZT-P09 specimen under a hydrostatic loading condition. The initiation of phase transformation is represented by a sudden increase in strains (ε_a – axial strain; $\varepsilon_{l\text{-parallel to poling}}$ – lateral strain parallel to poling direction, $\varepsilon_{l\text{-normal to poling}}$ – lateral strain perpendicular to poling direction, and volumetric strain ε_v).

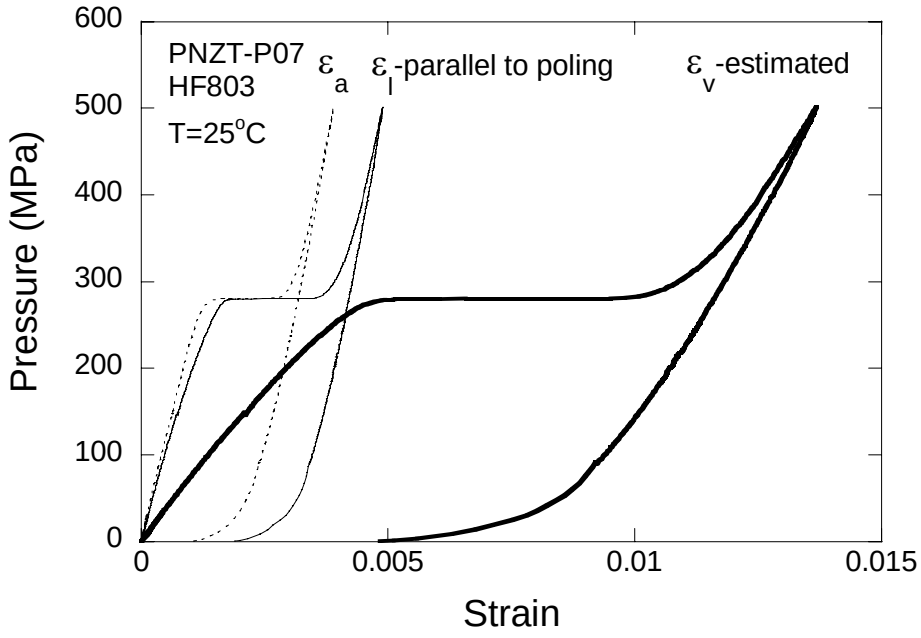

Figure 7. Phase transformation in the poled "chem-prep" PNZT-P07 specimen under a hydrostatic loading condition. The initiation of phase transformation is represented by a sudden increase in strains (ε_a – axial strain; $\varepsilon_{l\text{-parallel to poling}}$ – lateral strain parallel to poling direction, and estimated volumetric strain $\varepsilon_{v\text{-estimated}} = \varepsilon_a + 2\varepsilon_{l\text{-parallel to poling}}$).

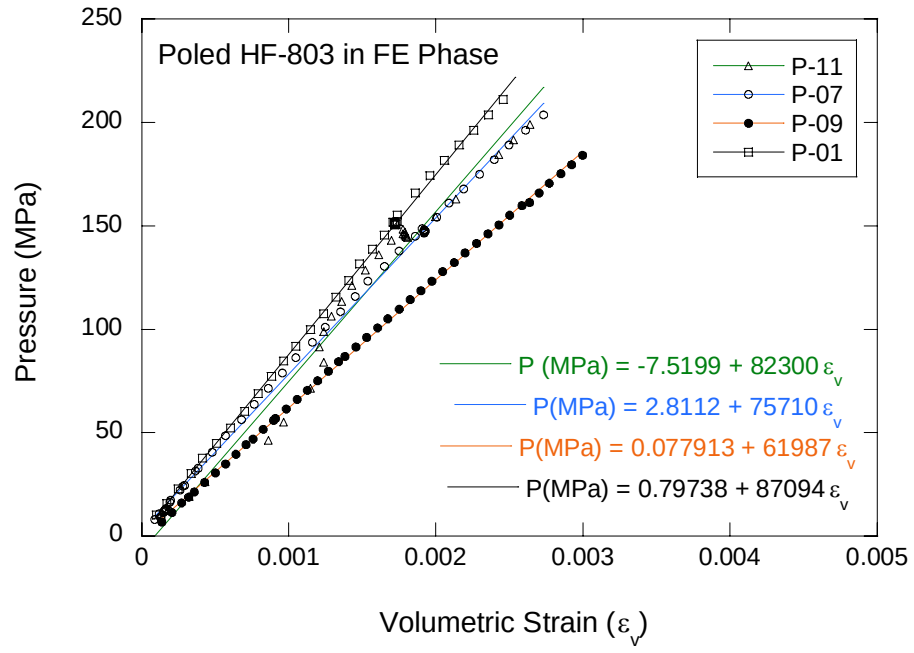

Figure 8. Bulk moduli of the poled "chem-prep" PNZT HF803 ceramic under the hydrostatic compression loading condition – FE phase data only.

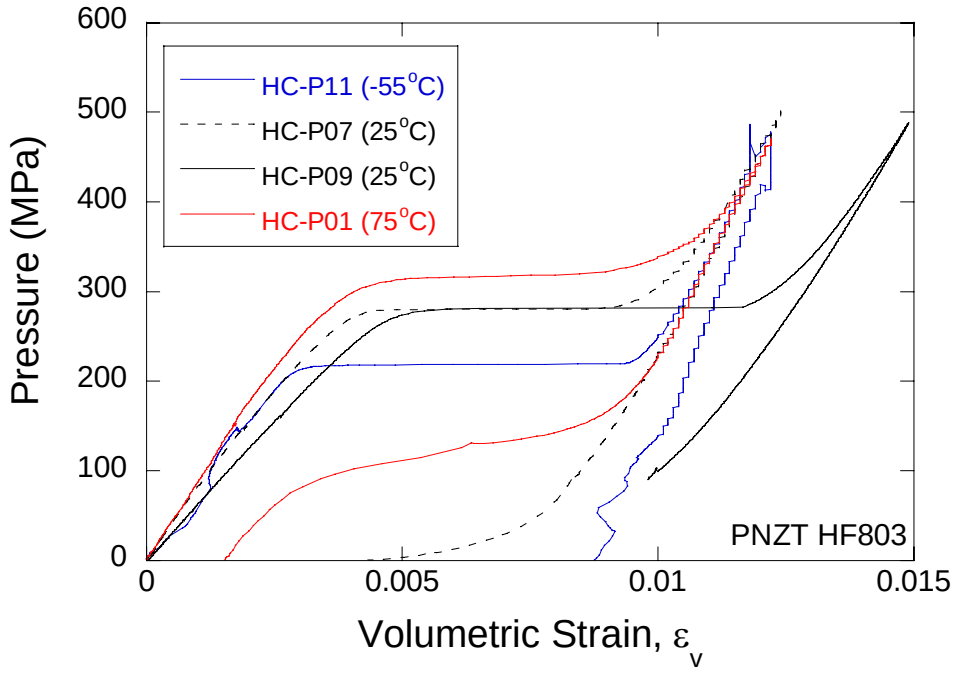

Figure 9. Superimposed Pressure vs. Volumetric strain (ε_v) plots for the hydrostatic compression tests on poled PNZT-HF803 specimens at temperatures of –55, 25, and 75°C.

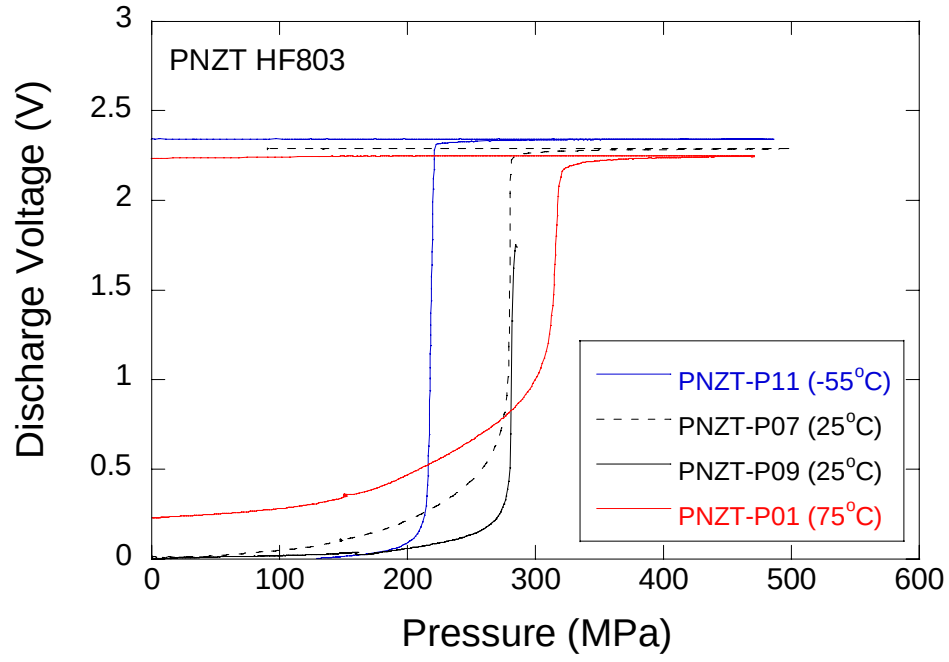

Figure 10. Superimposed Discharge voltage vs. Pressure plots for hydrostatic compression tests on poled PNZT-HF803 specimens at temperatures of –55, 25, and 75°C.

Figure 8 shows P vs. $\varepsilon_{v\text{-corrected}}$ plots obtained from the hydrostatic compression of poled HF803 specimens at pressures below the FE-to-AFE phase transformation. The slope for each curve (shown as the leading coefficient of the ε_v term in Figure 8) determines the bulk modulus of the ceramic in the FE phase.

$$K_{FE}=P / \varepsilon_{v\text{-corrected}} \qquad (2)$$

Figures 9 and 10 show the effects of temperature on the depoling pressures (P_T^H) of the poled HF803 ceramic. At high temperature, the phase transformation was reversible from AFE to FE, whereas at low temperature, the FE-to-AFE transition was permanent, i.e., the ceramic did not revert to the FE phase even after the hydrostatic pressure that caused the phase transformation had been removed. Electro-mechanical response of the PNZT observed from the Discharge Voltage vs. P plot (Figure 10) can be used to confirm the validity of the P_T^H values observed in the P vs. ε_v plot (Figure 9). Figures 9 and 10 confirm that sudden increases in volumetric strain and in discharge voltage are observed at the identical depoling pressure, P_T^H. Figure 10 also shows that the rate of discharging voltages is retarded as the temperature increases. The retarding effect of temperature is quantitatively shown in Figure 11, which displays discharge rate (dV/dP) vs. pressure. Figure 11 clearly shows that as the temperature increases the discharge rate decreases and the retardation in kinetics of phase transformation increases. Similar phenomena have been reported for different batches of "mixed-oxide" ceramic under increasing shear stresses (Zeuch *et al.*, 1999a). Qualitatively speaking, the effect of temperature on the phase transformation phenomenon appears to be analogous to the effect of shear stress.

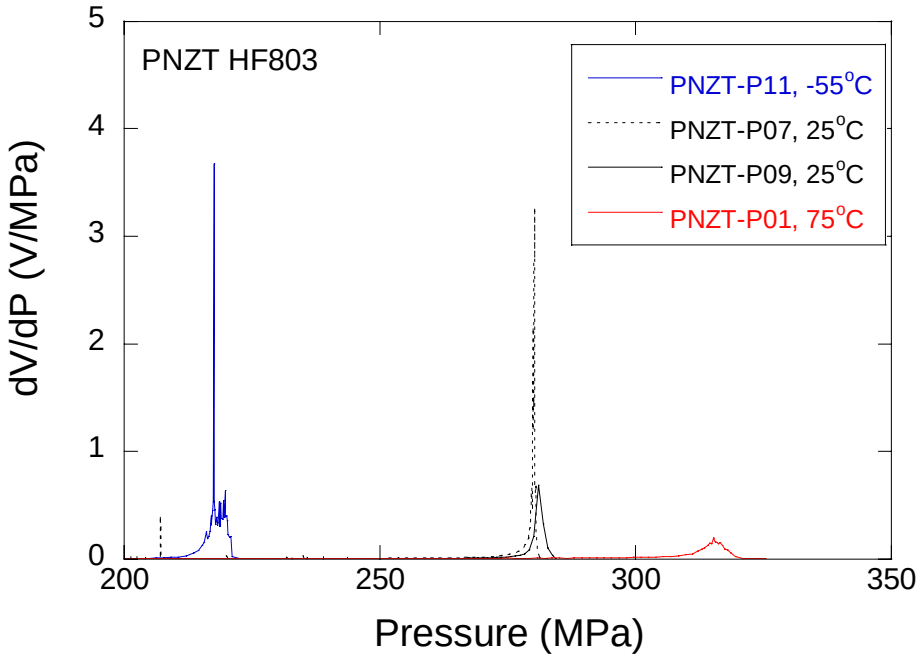

Figure 11. Discharge rate of the poled PNZT HF803 ceramic for temperatures of –55, 25, and 75°C.

Table 2 summarizes the results from the hydrostatic compression of the poled "chem-prep" PNZT HF803 ceramic at different temperatures. Individual depoling pressures (P_T^H), the volumetric strain corresponding to P_T^H, and bulk moduli determined from the FE phase for the poled "chem-prep" characterize the electro-mechanical response of the poled PNZT HF803 ceramic. The results from our earlier tests on unpoled PNZT HF803 are also presented in this table for comparison. Table 2 and Figure 12 show a comparison of P_T^H for the FE-to-AFE phase transformation in poled and unpoled ceramics. Variations of P_T^H with respect to temperature are well represented by two best-fit straight lines:

$$P_p^H \text{ (MPa)} = 261 + 0.74\ T\ (^oC) \quad (3)$$

$$P_u^H \text{ (MPa)} = 227 + 0.76\ T\ (^oC) \quad (4)$$

where P_u^H and P_p^H are the unpoled and poled phase transformation pressures in MPa, respectively, and T is temperature in °C.

The rates of increase in the phase transformation pressures (0.74 MPa/°C for the poled ceramic and 0.76 MPa/°C for the unpoled ceramic) were practically identical for both unpoled and poled PNZT HF803 specimens. For 100°C temperature changes, the differences ($P_p^H - P_u^H$) caused by the rate changes will be only 2 MPa. The real difference between equations (3) and (4) is the 34 MPa offset at T=0°C. This increase in depoling pressure for the poled ceramic compared to the unpoled ceramic is of the same magnitude (40 MPa) as reported for PNZT HF424 (Zeuch *et al.*, 1995). The difference is caused by the energy difference between the FE and AFE states caused by the work done during the poling process (Zeuch *et al.*, 1995).

The results described above are consistent with previous observations on specimens of unpoled "mixed-oxide" PNZT ceramic from batch HF453 tested under quasi-static conditions using the hydrostatic loading path. However, we reported a discrepancy between the "chem-prep" HF803 and the "mixed-oxide" HF453 in the properties of K_{FE} obtained from the hydrostatic loading (Lee *et al.*, 2003). The larger of the two values of K_{FE} (~80 GPa at room temperature) observed for HF803 compared to the HF453 value (~ 64 GPa) was attributed possibly to the HF803 material being in a mixed phase, i.e. having both FE and AFE phases present (Zeuch *et al.*, 1999c). Table 2 indicates that average K_{FE} value for the material from the poled HF803 is about 70 MPa. The reduction in K_{FE} for the poled ceramic is expected because the poling process under an electric field induces material in the AFE phase to transform to the FE phase. Hence, the poled material should have a larger mass fraction in the FE phase than the unpoled ceramic. Because of the small number of poled ceramic tests at each temperature, we could not make any definite conclusions regarding the impact of different processes on the stiffness of the PNZT ceramic represented by K_{FE}. The variations in bulk modulus in poled HF803 should be investigated further if HF803 specimens are available in the future.

Table 2. Summary of phase transformation in "chem-prep" PNZT-HF803 under hydrostatic compression (HC).

Specimen no.	Polarization	Temperature (°C)	K_{FE} (GPa)	ε_{vT}	P_T^H (MPa)
PNZT-P11	Poled	-55	82	0.0030	219
PNZT-P07	Poled	25	76	0.0041	281
PNZT-P09	Poled	25	62	0.0047	281
PNZT-P01	Poled	75	87	0.0040	314
PNZT-52	Unpoled	-55	115	0.0016	189
PNZT-64	Unpoled	-45	104	0.0019	196
PNZT-63	Unpoled	-35	103	0.0019	199
PNZT-53	Unpoled	-25	94	0.0021	200
PNZT-57	Unpoled	-15	92	0.0023	216
PNZT-58	Unpoled	-10	91	0.0025	224
PNZT-59	Unpoled	-5	90	0.0025	225
PNZT-55	Unpoled	5	86	0.0026	226
PNZT-65	Unpoled	15	81	0.0029	236
PNZT-34	Unpoled	25	84	0.0029	248
PNZT-45	Unpoled	41	81	0.0031	251
PNZT-44	Unpoled	58	83	0.0032	270
PNZT-60	Unpoled	75	87	0.0033	291

K_{FE} - bulk modulus in FE (ferroelectric) phase
P_T^H - pressure for FE-to-AFE phase transformation under hydrostatic compression
ε_{vT} - volumetric strain at P_T

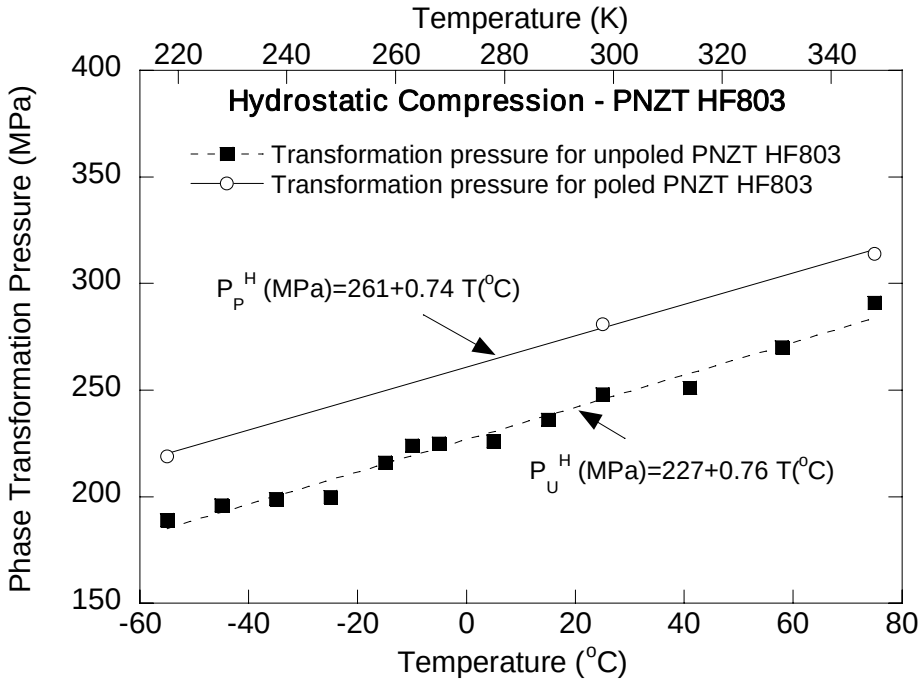

Figure 12. Variations of phase transformation pressures (P_P^H for poled and P_U^H for unpoled ceramic) in PNZT HF803 as a function of temperature.

3.2 Unconfined uniaxial compression test

To study the effect of mean stress (σ_m) and the major principal stress (σ_1) on the FE-to-AFE phase transformation in poled "chem-prep" PZT HF803, we carried out four uniaxial compression (UC) tests at temperatures of -55, 25 and 75°C. The specimens were prepared in the identical parallelepiped shape using the specifications described for hydrostatic compression test specimens. A temperature-controlled environmental chamber was modified to fit a 0.1 MN servo-controlled loading machine. The instrumented specimen was placed between the upper and the lower loading pistons and loaded until it failed. The axial load (σ_a) was applied at rate of about 2 MPa/s resulting from the stroke control of the loading machine at 0.025 mm/s. In three UC tests, ε_a and $\varepsilon_{l\text{-parallel to poling}}$ were measured from two pairs of axial and lateral strain gages. In the PNZT P-21 test, an additional pair of lateral strain gages was used to measure $\varepsilon_{l\text{-normal to poling}}$. The stress-strain records from all UC tests are shown in Appendix B. Figure 13 shows a stress vs. strain plot obtained from the uniaxial compression test of the PNZT-12 specimen. The major principal stress applied along the long axis of the specimen is plotted against ε_a and $\varepsilon_{l\text{-parallel to poling}}$, respectively. The discharge voltage is also plotted against the major principal stress to correlate the phase transformation stress level with that determined from the stress-strain behavior of the specimen. The failure of the specimen is indicated by the peak stress (510 MPa) shown for the stress-strain curve.

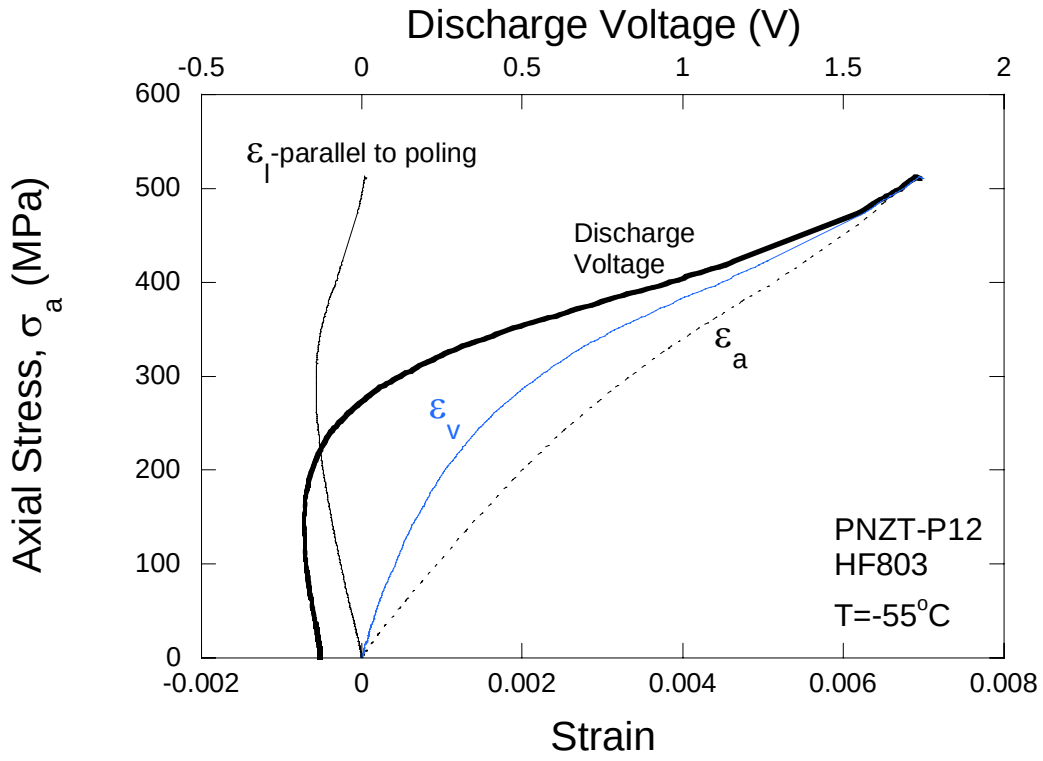

Figure 13. Typical uniaxial compression test on poled PNZT-HF803 ceramic. The major principal stress acting in the direction of the long axis of the specimen (σ_1) is plotted against

axial (ε_a), lateral ($\varepsilon_{\text{l-parallel to poling}}$), and volumetric ($\varepsilon_v$) strains, respectively, and also against discharge voltage.

Unlike the distinctive phase transformation shown in previous sections that discussed the HC test results, strains and discharge voltage change very gradually as the axial stress (σ_a) is increased during the UC tests. Axial strain (ε_a) increases linearly with the axial stress until the phase transformation occurs as indicated by the gradual increase in discharge voltage. The lateral strain changes slope as a result of superposition of both dilatational lateral strains caused by the shear stress at low mean stress and the strains produced during the FE-to-AFE phase transformation. When the axial stress applied in the UC test approaches the pressure required for the phase transformation (P_P^H = 219 MPa at -55°C from Table 2) determined from the HC test, the poled ceramic appears to go through a phase transformation. Therefore, the overall maximum principal stress rather than the mean stress ($\sigma_1=\sigma_a\neq\sigma_m$) seems to be the controlling stress for phase transformation in PNZT. The discussion of the critical stress for phase transformation under general stress conditions will be detailed in the next section.

3.3 Constant stress difference test

To characterize the effects of shear stress on the polymorphic and depoling behaviors of the poled "chem-prep" PNZT HF803, a series of Constant-Stress-Difference (CSD) tests (Zeuch *et al.*, 1999a) was conducted for four stress differences (50, 100, 150, and 300 MPa) and three temperatures (-55, 25, and 75°C). The specimens were prepared according to the same procedure and specifications used for preparing the HC and UC specimens as described in previous sections. An example of the CSD loading path is shown in Figure 14. The PNZT-P08 specimen was loaded hydrostatically to about 70 MPa. This pressure is far below the expected depoling pressure (P_p^H ~219 MPa at -55°C) determined from the HC tests on the poled HF803 ceramic. With the confining pressure ($P=\sigma_3$) held constant, additional load was applied along the long axis of the specimen to create the stress difference ($\sigma_d = \sigma_1 - \sigma_3$). Then, both σ_1 and σ_3 were increased simultaneously at the same rate of 0.7 MPa/s to maintain the stress difference (σ_d) constant while increasing the mean stress (σ_m). Appendix C shows the loading paths used for all CSD testing, discharge voltage plots, and the stress-strain records with respect to the major and the minor principal stresses, respectively.

Figures 15 and 16 show the changes of ε_a and $\varepsilon_{\text{l-parallel to poling}}$ with respect to σ_3 and σ_1 for the CSD stress condition. As in the HC tests, the sudden increase (reduction in length) in ε_a and $\varepsilon_{\text{l-parallel to poling}}$ of the specimen indicated the FE-to-AFE transition. During the increase in σ_d to 300 MPa, ε_a increases (reduction in length) about 0.16 % and $\varepsilon_{\text{l-parallel to poling}}$ decreases about 0.05 %. These deformations are shown by horizontal lines in Figure 15 for constant σ_3 and by inclined lines in Figure 16 for increasing σ_1. Both plots show that the application of the 300 MPa stress difference resulted in a stress state well below the FE-to-AFE phase transformation stress state at -55°C. The subsequent increase of approximately 70 MPa, both in σ_1 and σ_3, triggered the transition of the polymorphic structure as indicated by the sudden reduction in volume.

Different levels of constant σ_d were applied for each temperature. Figures 17, 18, and 19 show the σ_1 vs. ε_a and σ_1 vs. $\varepsilon_{\text{l-parallel to poling}}$ plots for the CSD tests conducted at the three different test temperatures (low: -55°C, ambient: 25°C, and high: 75°C). A HC test record for the corresponding temperature is also included in the plots to compare the results from the CSD testing with the baseline ($\sigma_d = 0$) result obtained from the HC test. At each temperature, we observed a consistent increase of σ_d (or shear stress) for increasing σ_{1T}^{CSD}, the maximum principal stress required for FE-to-AFE phase transformation under CSD stress condition. We also noticed that increasing shear stress retarded the rate of transformation. At higher shear stress, the phase transformation becomes more gradual indicated by the increase in curvature of the plot at onset of transformation.

Table 3 summarizes the results from the CSD tests conducted on the poled PNZT HF803 ceramic. Results from the HC tests (PNZT-11, 7, and 1) are also shown to represent the baseline case (σ_d=0 MPa) for the CSD loading path. Table 3 also shows the effect of temperature on the critical stresses required for the phase transformation of the poled "chem-prep" PNZT-HF803. If we choose the tests conducted for the same stress difference (e.g. σ_d=100 MPa), both σ_{1T}^{CSD} and σ_{3T}^{CSD} (the minimum principal stress for FE-to-AFE phase transformation under CSD stress condition) increase about 90 MPa for the increase of 130°C in temperature. This rate of increase (0.7 MPa/°C) in the CSD condition is very close to the rate (0.74 MPa/°C) found in the HC condition.

Table 3. Summary of phase transformation in poled "chem-prep" PNZT-HF803 under Constant Stress Difference (CSD) loading.

Specimen no.	σ_d (MPa)	Temperature (^{0}C)	σ_{3T}^{CSD} (MPa)	σ_{1T}^{CSD} (MPa)	σ_m^{CSD} (MPa)
PNZT-P11	0	-55	219	219	219
PNZT-P16	50	-55	183	233	200
PNZT-P23	100	-55	205	305	238
PNZT-P08	300	-55	138	438	238
PNZT-P07	0	25	281	281	281
PNZT-P09	0	25	281	281	281
PNZT-P19	100	25	255	355	288
PNZT-P24	150	25	NA	NA	NA
PNZT-P01	0	75	314	314	314
PNZT-P22	50	75	NA	NA	NA
PNZT-P17	100	75	295	395	328
PNZT-P05	150	75	NA	NA	NA

σ_d - stress difference between the maximum (σ_1) and the minimum (σ_3) compressive stresses
σ_m^{CSD} - mean stress, $(\sigma_1 + 2\sigma_3) / 3$
σ_{1T}^{CSD} - maximum compressive stress for FE-to-AFE phase transformation under CSD compression
σ_{3T}^{CSD} - minimum compressive stress for FE-to-AFE phase transformation under CSD compression

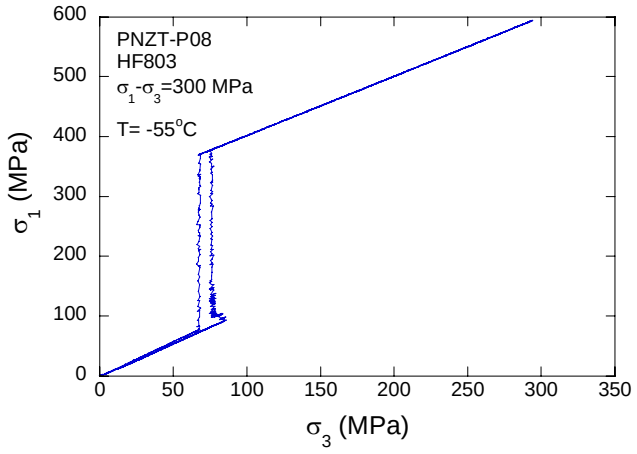

Figure 14. A loading path obtained from the Constant Stress Difference test in poled "chem-prep" PNZT-HF803 P08 specimen with 300 MPa stress difference ($\sigma_d=\sigma_1-\sigma_3$).

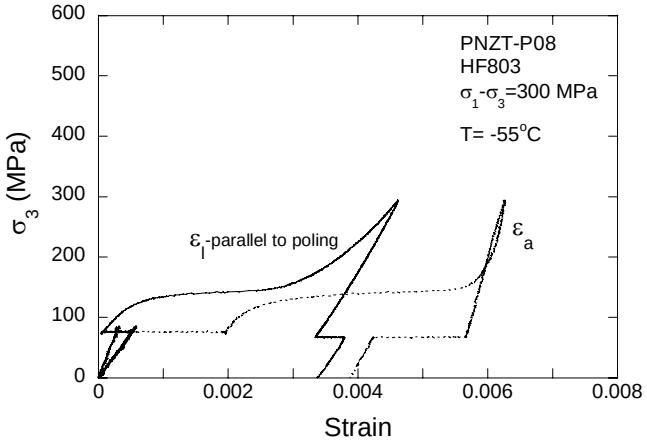

Figure 15. Minimum principal stress (σ_3) vs. strain response of the poled "chem-prep" PNZT-HF803 ceramic under the Constant Stress Difference condition. Phase transformation is represented by an increase in axial (ε_a) and lateral (ε_l) strains around 138 MPa of σ_3.

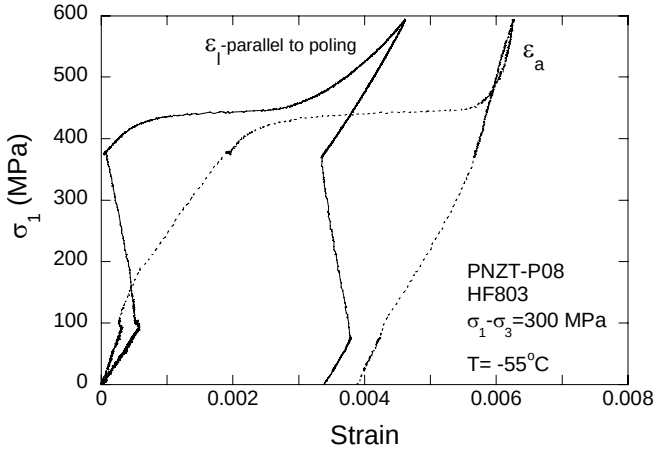

Figure 16. Maximum principal stress (σ_1) vs. strain response of the poled "chem-prep" PNZT-HF 803 ceramic under the Constant Stress Difference condition. Phase transformation is represented by an increase in axial (ε_a) and lateral (ε_l) strains around 438 MPa of σ_1.

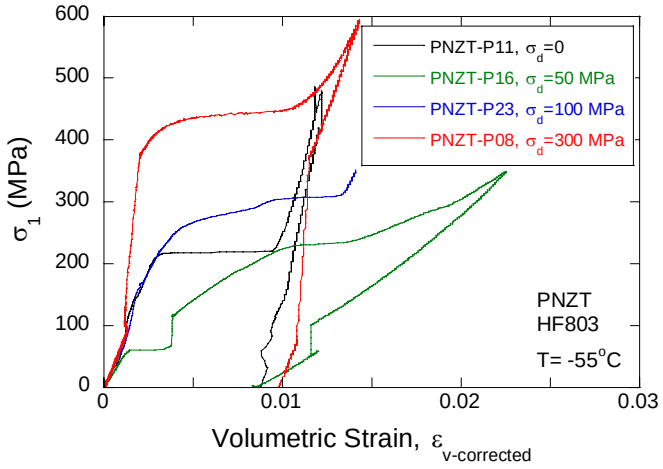

Figure 17. Effect of stress difference (σ_d) during phase transformation of the poled "chem-prep" PNZT-HF803 ceramic at low temperature (-55°C).

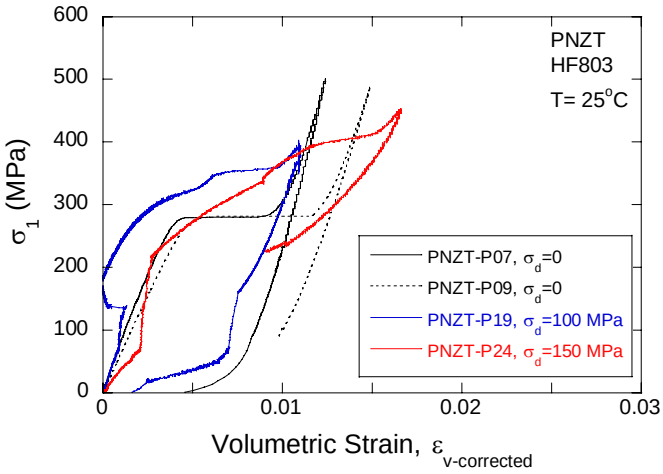

Figure 18. Effect of stress difference (σ_d) during phase transformation of the poled "chem-prep" PNZT-HF803 ceramic at ambient temperature (25°C).

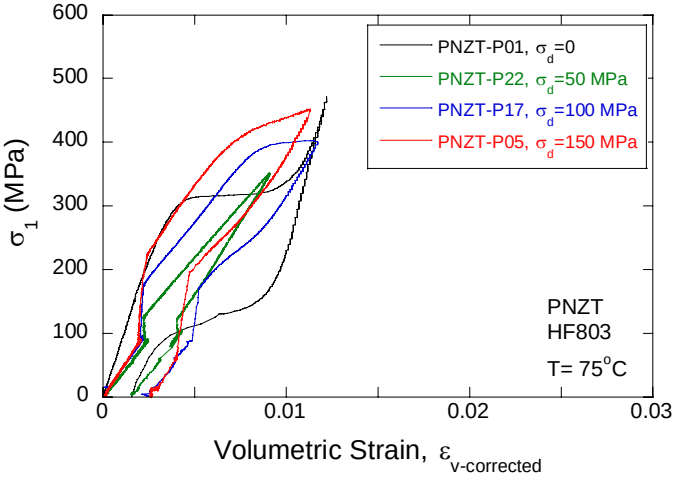

Figure 19. Effect of stress difference (σ_d) during phase transformation of the poled "chem-prep" PNZT-HF803 ceramic at elevated temperature (75°C).

From the earlier tests conducted on different unpoled ceramics such as PNZT HF541 (Zeuch *et al.*, 1992), HF424 (Zeuch *et al.*, 1994), and HF803 (Lee *et al.*, 2003), the FE-to-AFE transition criterion of the unpoled ceramic has been well established. Under the CSD stress condition, the FE-to-AFE phase transformation occured when the maximum compressive stress (σ_{1T}^{CSD}) equaled the hydrostatic pressure (P_u^H) at which the transition otherwise occurred.

$$\sigma_{1T}^{CSD} = P_u^H \tag{5}$$

This relationship can be rewritten in terms of the mean stress and the maximum principal stress (Zeuch *et al.*, 1999b).

$$\sigma_{mu}^{CSD} = P_u^H - \frac{2\sigma_d}{3} \tag{6}$$

Comparisons of equations (5) and (6) show that for a CSD test of unpoled ceramic the mean phase transformation stress (σ_{mu}^{CSD}) is less than the maximum principal transformation stress (σ_{1T}^{CSD}) by a factor equal to two-thirds of the stress difference (σ_d).

However, due to a preferential crystallographic orientation caused by dipole rotation associated with poled ceramics, not only the magnitude of σ_{1T}^{CSD} but also its directional relationship to the crystallographic plane about the polar axis becomes important. Figure 20 shows a schematic of a poled ceramic specimen under the triaxial stress condition ($\sigma_1 > \sigma_2 = \sigma_3$).

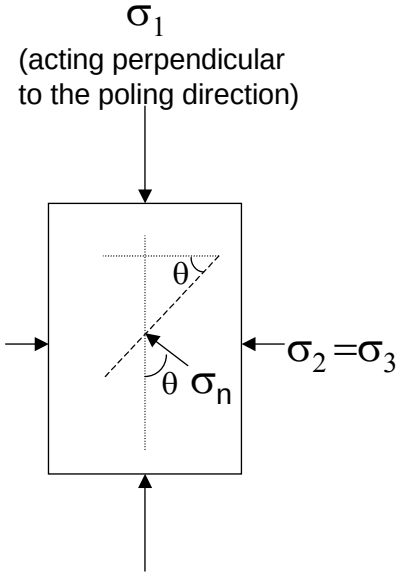

Figure 20. Schematic of a poled ceramic under triaxial stress conditions. σ_1, σ_2, and σ_3 are the maximum, intermediate, and minimum principal stresses, respectively. σ_n is the stress acting normal to the crystallographic plane dipping θ from the poling direction.

We assume that the transformation occurs when the normal compressive stress (σ_n) reaches the hydrostatic pressure (P_T^H) at which the FE-to-AFE transformation would otherwise take place.

$$\sigma_n = \frac{\sigma_1 + \sigma_3}{2} + \frac{\sigma_1 - \sigma_3}{2}\cos 2\theta \tag{7}$$

$$\sigma_n = P_T{}^H \tag{8}$$

Then, the maximum principal stress (σ_{1T}^{CSD}) at the FE-to-AFE transformation can be represented in terms of the stress difference (σ_d).

$$P_T{}^H = \frac{\sigma_{1T}^{CSD} + \sigma_{3T}^{CSD}}{2} + \frac{\sigma_{1T}^{CSD} - \sigma_{3T}^{CSD}}{2}\cos 2\theta \tag{9}$$

$$P_T{}^H = \frac{\sigma_{1T}^{CSD} + (\sigma_{1T}^{CSD} - \sigma_d)}{2} + \frac{\sigma_d}{2}\cos 2\theta \tag{10}$$

$$\sigma_{1T}^{CSD} = P_T^H + \frac{1 - \cos 2\theta}{2}\sigma_d \tag{11}$$

Equation (11) is a general formula of phase transformation both for the unpoled and for the poled ceramic. For an unpoled ceramic, no preferential crystallographic plane exists about the polar axis. Therefore, some crystallographic plane exists along the long axis of the specimen, oriented perpendicular to σ_1 (or $\theta = 0$). Thus, the following FE-to-AFE criterion for the unpoled ceramic is derived from the general criterion shown in equation (11).

$$\sigma_{1T}^{CSD} = P_u^H \tag{12}$$

Equation (12) confirms the earlier experimental results (Zeuch *et al.*, 1999a): phase transformation from FE to AFE occurs in unpoled ceramic when the maximum compressive stress equals the hydrostatic pressure at which the transformation otherwise takes place. For a poled ceramic, however, a preferential crystallographic plane ($\theta \neq 0$) exists about the polar axis. Thus, the general criterion as shown in equation (11) becomes the following phase transformation criterion for the poled ceramic.

$$\sigma_{1T}^{CSD} = P_p^H + \frac{1 - \cos 2\theta}{2}\sigma_d \tag{13}$$

Resolution of a normal stress equal to P_p^H on a plane dipping at an angle θ from the poling direction requires a maximum compressive stress σ_{1T}^{CSD} that is greater than P_p^H by $\frac{1-\cos 2\theta}{2}\sigma_d$. Figure 21 shows the maximum transformation stress (σ_{1T}^{CSD}) plotted against the stress difference (σ_d). As predicted in the unpoled criterion shown as equation (12), σ_{1T}^{CSD} for the unpoled PNZT HF803 is P_u^H at $\sigma_d = 0$. Even though σ_d increases to 200 MPa, σ_{1T}^{CSD} is rather consistent maintaining the value of P_u^H. For the poled ceramic, our experimental result confirms the poled criterion suggested in equation (13). At all temperatures (-55, 25, and 75°C) investigated in our tests, σ_{1T}^{CSD} varied linearly with σ_d (see Figure 21). The slopes of these straight lines were about 0.75.

$$\frac{1-\cos 2\theta}{2} = 0.75 \qquad (13)$$

Therefore, the angle θ for the poled "chem-prep" PNZT HF803 was about 60°. The linear relationships of σ_{1T}^{CSD} with respect to σ_d shown in Figure 21 clearly indicate that the FE-to-AFE phase transformation occurs in the poled PNZT ceramic when the normal compressive stress (σ_n) acting perpendicular to a crystallographic plane, dipping □ from the poling direction, reaches the hydrostatic pressure at which transformation would otherwise take place.

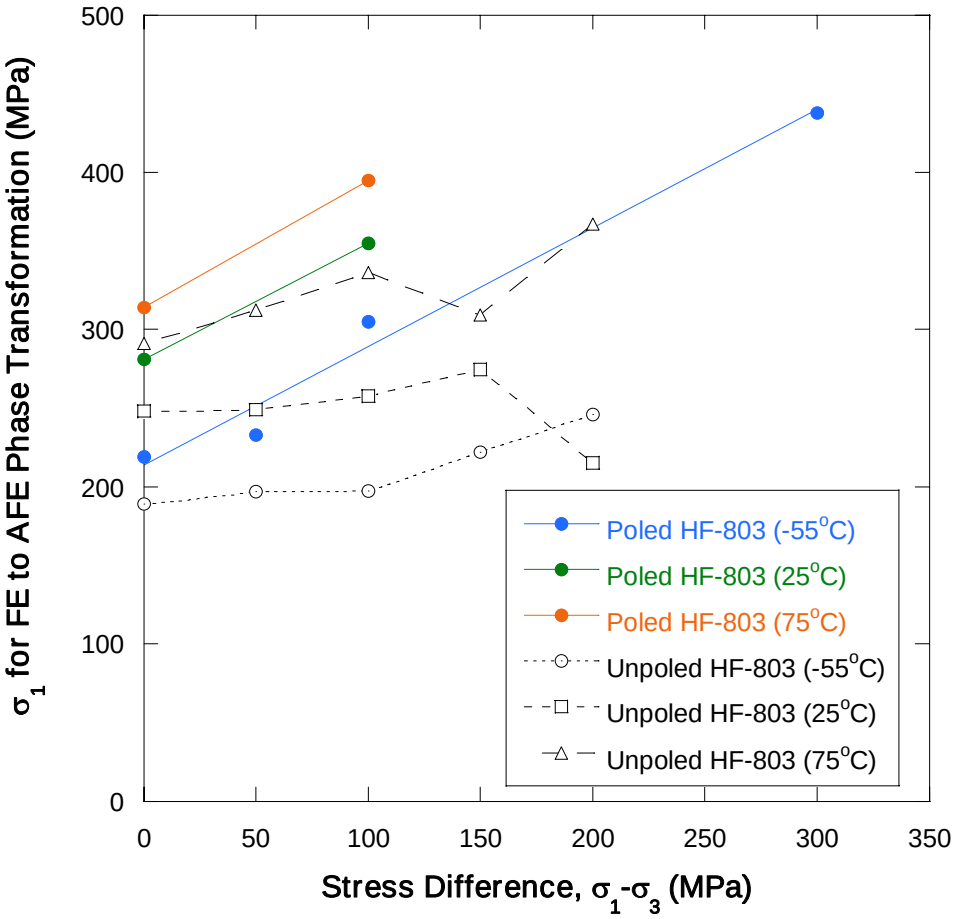

Figure 21. The maximum principal stress required for FE-to-AFE phase transformation as a function of stress difference.

4. Conclusions

The specimens of poled "chem-prep" PNZT ceramic from batch HF803 were tested under three different quasi-static loading conditions: hydrostatic compression, uniaxial compression, and constant stress difference compression. The electro-mechanical behavior during phase transformation from a ferroelectric rhombohedral perovskite structure (FE) to an antiferroelectric orthorhombic (AFE) structure was investigated at three temperatures (-55, 25, and 75°C). The results from the laboratory experiments are summarized as follows:

- FE-to-AFE phase transformation occurs in the poled PNZT ceramic when the normal compressive stress (σ_n) acting perpendicular to a crystallographic plane dipping □ from the poling direction, equals the hydrostatic pressure (P_p^H) at which the transformation otherwise takes place. This criterion can be represented in terms of the maximum principal stress (σ_{1T}^{CSD}) at transformation and the stress difference (σ_d):

$$\sigma_{1T}^{CSD} = P_p^H + \frac{1-\cos 2\theta}{2}\sigma_d$$

- Under a hydrostatic loading condition, the FE-to-AFE phase transformation pressure (P_p^H) for the poled "chem-prep" PNZT HF803 ceramic heated to different temperatures is represented by the following linear relationship:

$$P_p^H \text{ (MPa)} = 260 + 0.73 \text{ T (°C)}$$

- The poled "chem-prep" PNZT HF803 ceramic undergoes anisotropic deformation during the transition from a FE to an AFE structure. The lateral strain parallel to the poling direction ($\varepsilon_{\text{l-parallel to poling}}$) is typically 35% greater than the strain perpendicular to the poling direction ($\varepsilon_{\text{l-normal to poling}}$).

- The retarding effect of temperature on the kinetics of phase transformation appears to be analogous to the effect of shear stress.

References

Bauer, F., K. Vollrath, Y. Fetiveau and L. Eyraud (1976), *Ferroelectric ceramics: application to mechanical energy conversion under shock compression*, Ferroelectrics, **10**: 61-64.

Brannon, R. M., Montgomery, S. T., Aidun, J. B., and A. C. Robinson (2001), *Macro- and meso-scale modeling of PZT ferroelectric ceramics*, 12th Biennial International Conference of the American Physical Society Topical Group on Shock Compression on Condensed Matter, Atlanta, GA.

Fritz, I. J., and J. D. Keck (1978), *Pressure-temperature phase diagrams for several modified lead zirconate ceramics*, J. Phys. Chem. Solids, **39**: 1163-1167.

Fritz, I. J. (1979), *Stress effects in two modified lead zirconate titanate ferroelectric ceramics*, J. Appl. Phys. **50** (8): 5265-5271.

Lee, M. Y. (2004), *Characterization of "chem-prep" PZT HF1035*, FY04 mid-year review presentation at C-6 conference, Albuquerque, NM.

Lee, M. Y., Montgomery, S. T., Hofer, J. H. and D. H. Zeuch (2003), *Hydrostatic, uniaxial, and triaxial compression tests on unpoled "Chem-prep" PZT 95/5-2Nb ceramic within temperature range of -55 to 75°C*, Rept. No. SAND2003-3651, Sandia National Laboratories, Albuquerque, NM.

Lysne, P. C. and C. M. Percival (1975), *Electric energy generation by shock compression of ferroelectric ceramics: normal-mode response of PZT 95/5*, J. Appl. Phys., **46**: 1519-1526.

Montgomery, S. T, Brannon, R. M., Robbins, J. H., Setchell, R. E., and D. H. Zeuch (2001), *Simulation of the effects of shock stress and electrical field strength on shock-induced depoling of normally poled PZT 95/5*, SAND2001-1734, Proc.12th Biennial International Conference of the APS Topical Shock Group on Shock Compression of Condensed Matter, June 24-29, Atlanta, GA.

Montgomery, S. T. and D. H. Zeuch (2004), *A model for the bulk mechanical response of porous ceramics exhibiting a ferroelectric-to-antiferroelectric phase transition during hydrostatic compression*, SAND2003-4560C, Proc. 28th International Cocoa Beach Conference and Exposition on Advanced Ceramics and Composites, January 25-30, Cocoa Beach, FL.

Voigt, J.A., Sipola, D. L., Tuttle, B. A. and M. T. Anderson (1999), *Nonaqueous solution synthesis process for preparing oxide powders of lead zirconate titanate and related materials*, U. S. Patent 5,908,802.

Yang, P. (2003), Personal communication.

Yang, P., Moore, R. H., Lockwood, S. J., Tuttle, B. A., Voigt, J. A., and T. W. Scofield (2003), *Chem-prep PZT 95/5 for neutron generator applications: the effect of pore former type*

and density on the depoling behavior of chemically prepared PZT 95/5 ceramics, Rept. No. SAND2003-3866, Sandia National Laboratories, Albuquerque, NM.

Zeuch, D. H., Montgomery, S. T., and J. D. Keck (1992), *Hydrostatic and triaxial compression experiments on unpoled PZT 95/5-2Nb ceramic: The effects of shear stress on the $F_{RI} \rightarrow A_O$ polymorphic phase transformation*, J. Mater. Res., **7**: 3314-3332.

Zeuch, D. H., Montgomery, S. T., and J. D. Keck (1994). *Further observations on the effects of nonhydrostatic compression on the $F_{RI} \rightarrow A_O$ polymorphic phase transformation in niobium-doped, lead-zirconate-titanate ceramic*, J. Mater. Res., **9**: 1322-1327.

Zeuch, D. H., Montgomery, S. T., Carlson, L. W. and D. J. Zimmerer (1995), *The effects of non-hydrostatic compression and applied electric field on the electromechanical behavior of poled PZT 95/5-2Nb ceramic during the $F_{RI} \rightarrow A_O$ polymorphic phase transformation*, Rept. No. SAND95-1951, Sandia National Laboratories, Albuquerque, NM.

Zeuch, D. H., Montgomery, S. T., and D. J. Holcomb (1999a), *The effects of nonhydrostatic compression and applied electric field on the electromechanical behavior of poled lead zirconate titanate 95/5-2Nb ceramic during the ferroelectric to antiferroelectric polymorphic transformation*, J. Mater. Res., **14**: 1814-1827.

Zeuch, D. H., Montgomery, S. T., Holcomb, D. J., Grazier, J. M., and L. W. Carlson (1999b), *Uniaxial compression experiments on PZT 95/5-2Nb ceramic: evidence for an orientation-dependent "maximum compressive stress" criterion for onset of the $F_{RI} \rightarrow A_O$ polymorphic phase transformation.* Rept. No. SAND99-0077, Sandia National Laboratories, Albuquerque, NM.

Zeuch, D. H., Montgomery, S. T., Carlson, L. W., and J. M. Grazier (1999c), *Failure surfaces and related mechanical properties for poled and unpoled PZT 95/5-2Nb voltage bar ceramic*, Rept. No. SAND99-0635, Sandia National Laboratories, Albuquerque, NM.

Zeuch, D. H., Lee, M. Y., Costin, L. S., Wawersik, W. R., Grazier, J. M., Bronowski, D. R., and R. D. Hardy (1999d), *A high-pressure, low-temperature triaxial test apparatus*, International Mechanical Engineering Congress & Exposition of the ASME. Nashville, TN.

APPENDIX A

Hydrostatic Compression (HC) Test Plots for Poled PNZT-HF803 (σ_a-axial stress, ε_a-axial strain, $\varepsilon_{l\text{-parallel to poling}}$-lateral strain parallel to poling direction, $\varepsilon_{l\text{-normal to poling}}$-lateral strain perpendicular to poling direction, $\varepsilon_{v\text{-estimated}}$-estimated volumetric strain, and T-temperature)

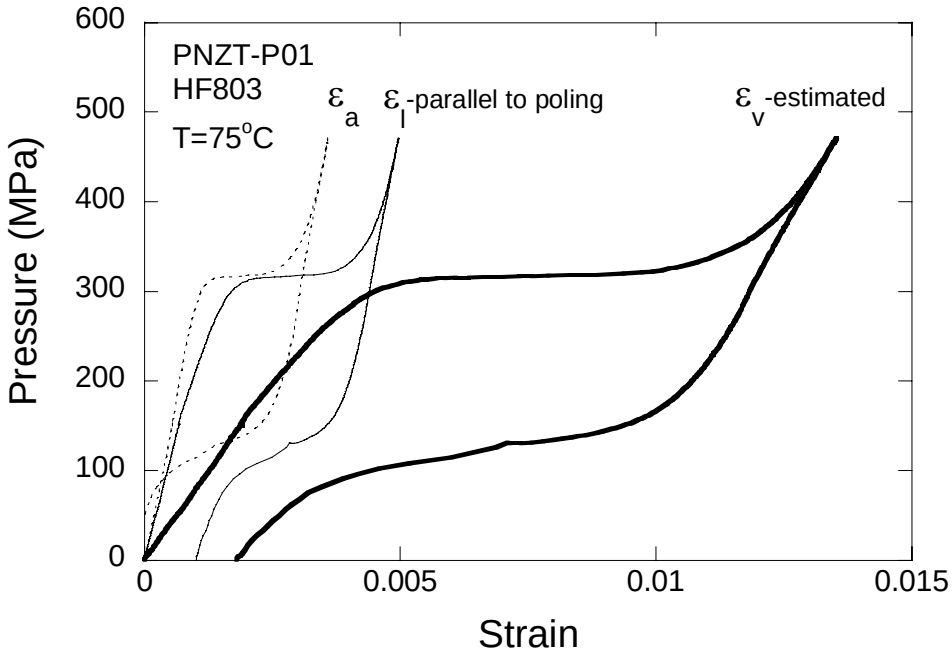
PNZT-P01
HF803
T=75°C
ε a
ε l -parallel to poling
ε v -estimated
Pressure (MPa)
Strain
600
500
400
300
200
100
0
0
0.005
0.01
0.015

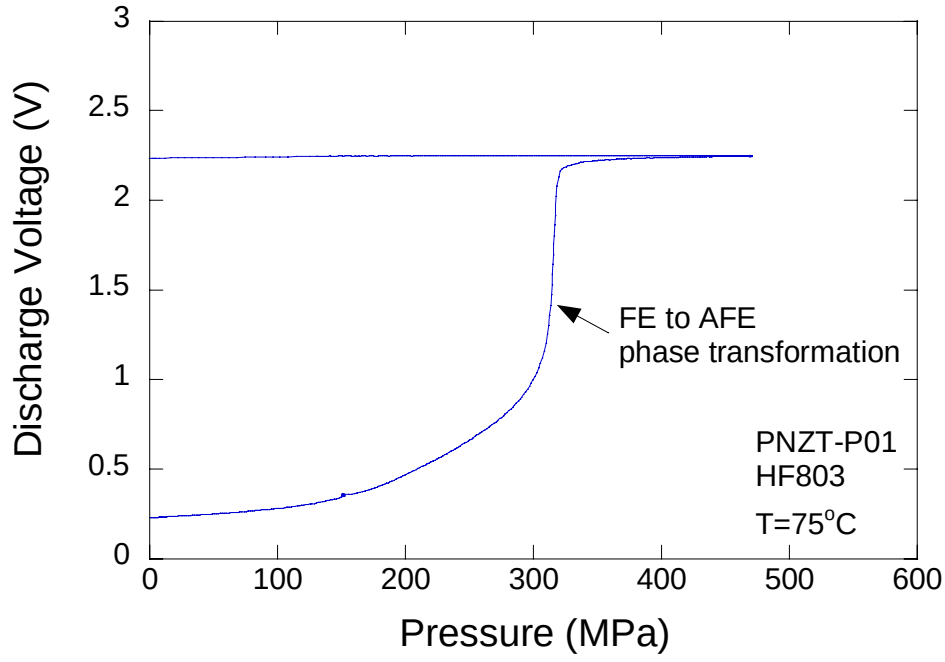
Discharge Voltage (V)
Pressure (MPa)
FE to AFE
phase transformation
PNZT-P01
HF803
T=75°C
3
2.5
2
1.5
1
0.5
0
0
100
200
300
400
500
600

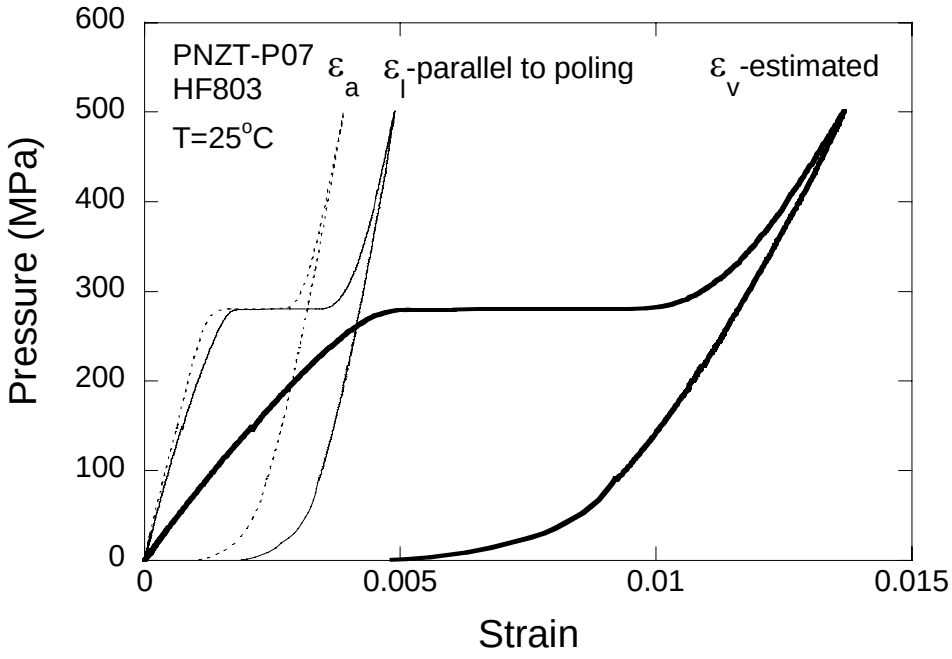
PNZT-P07
HF803
T=25°C
ε_a
ε_l-parallel to poling
ε_v-estimated
Pressure (MPa)
Strain
600
500
400
300
200
100
0
0
0.005
0.01
0.015

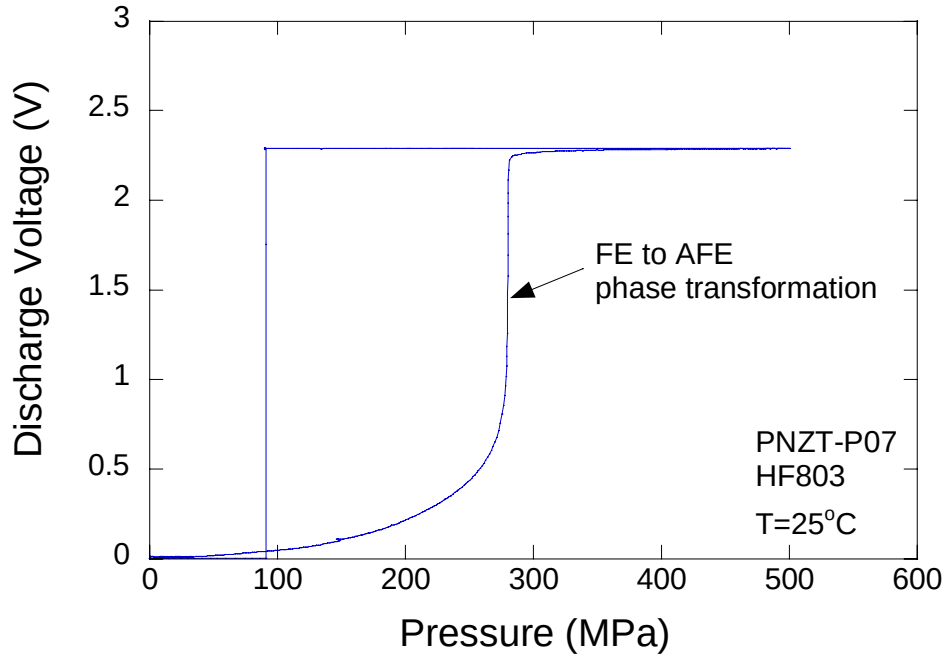
Discharge Voltage (V)
Pressure (MPa)
FE to AFE
phase transformation
PNZT-P07
HF803
T=25°C
3
2.5
2
1.5
1
0.5
0
0
100
200
300
400
500
600

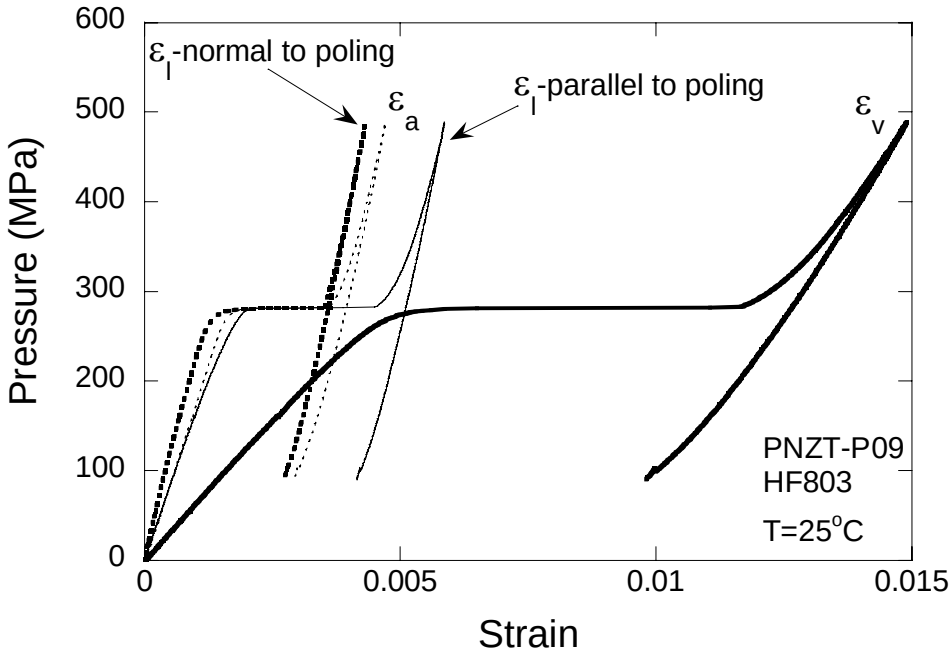
600
500
400
300
200
100
0
Pressure (MPa)
0
0.005
0.01
0.015
Strain
ε_l-normal to poling
ε_a
ε_l-parallel to poling
ε_v
PNZT-P09
HF803
T=25°C

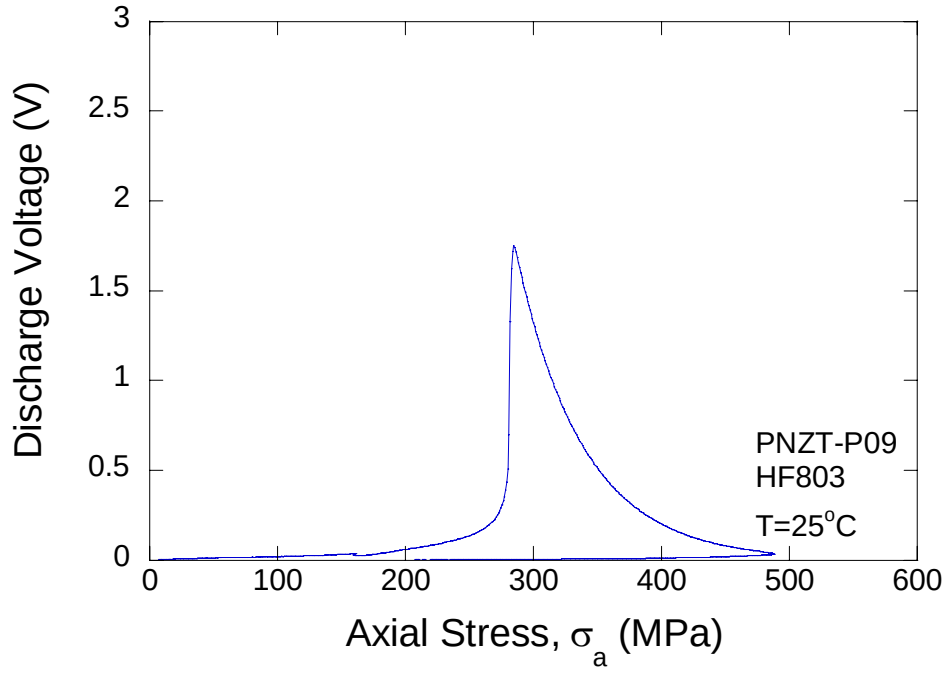
3
2.5
2
1.5
1
0.5
0
Discharge Voltage (V)
0
100
200
300
400
500
600
Axial Stress, σ_a (MPa)
PNZT-P09
HF803
T=25°C

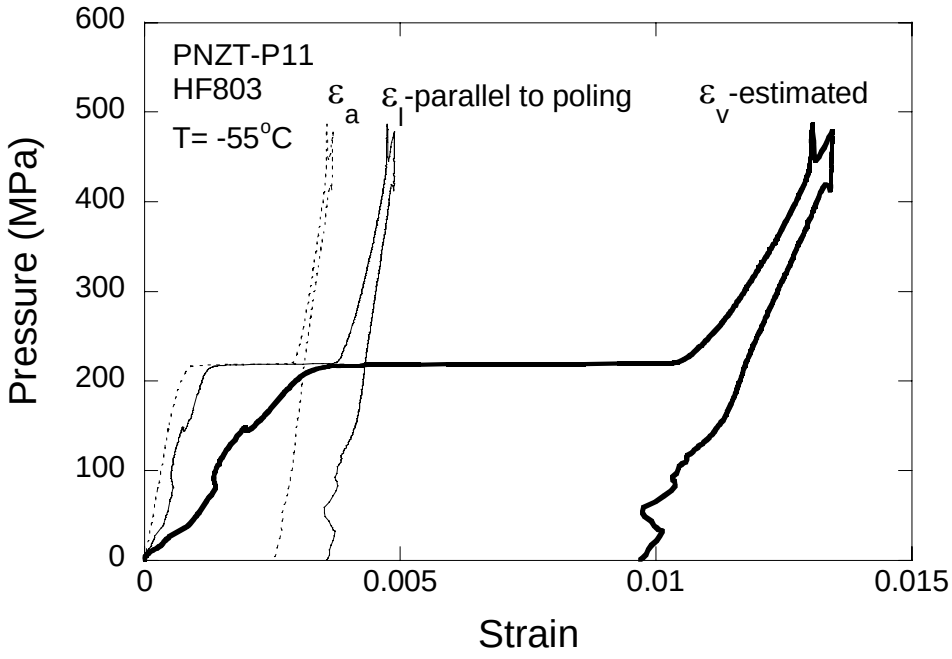
PNZT-P11
HF803
T= -55°C
ε_a
ε_l-parallel to poling
ε_v-estimated
Pressure (MPa)
Strain
600
500
400
300
200
100
0
0
0.005
0.01
0.015

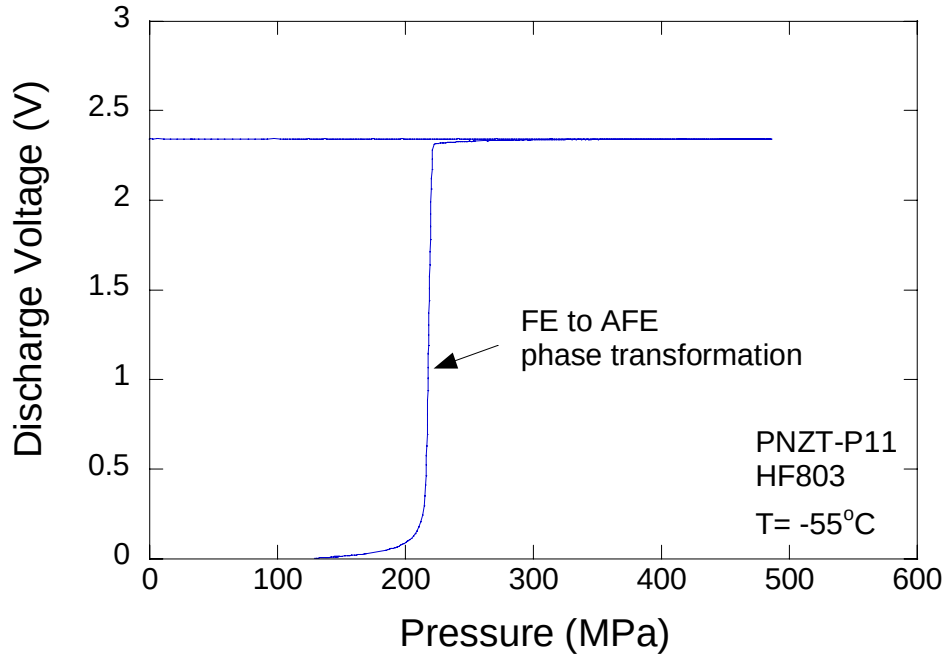
Discharge Voltage (V)
Pressure (MPa)
FE to AFE
phase transformation
PNZT-P11
HF803
T= -55°C
3
2.5
2
1.5
1
0.5
0
0
100
200
300
400
500
600

APPENDIX B

Uniaxial Compression (UC) Test Plots for Poled PNZT-HF803 (σ_a-axial stress, ε_a-axial strain, $\varepsilon_{l\text{-parallel to poling}}$-lateral strain parallel to poling direction, $\varepsilon_{l\text{-normal to poling}}$-lateral strain perpendicular to poling direction, and T-temperature)

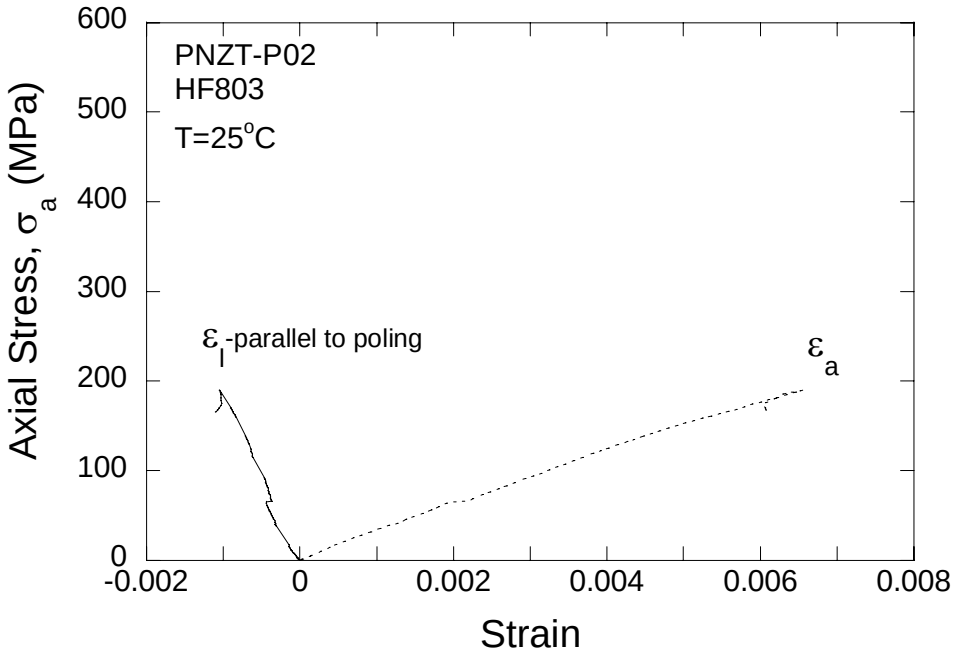
PNZT-P02
HF803
T=25°C
Axial Stress, σa (MPa)
εl-parallel to poling
εa
Strain
600
500
400
300
200
100
0
-0.002
0
0.002
0.004
0.006
0.008

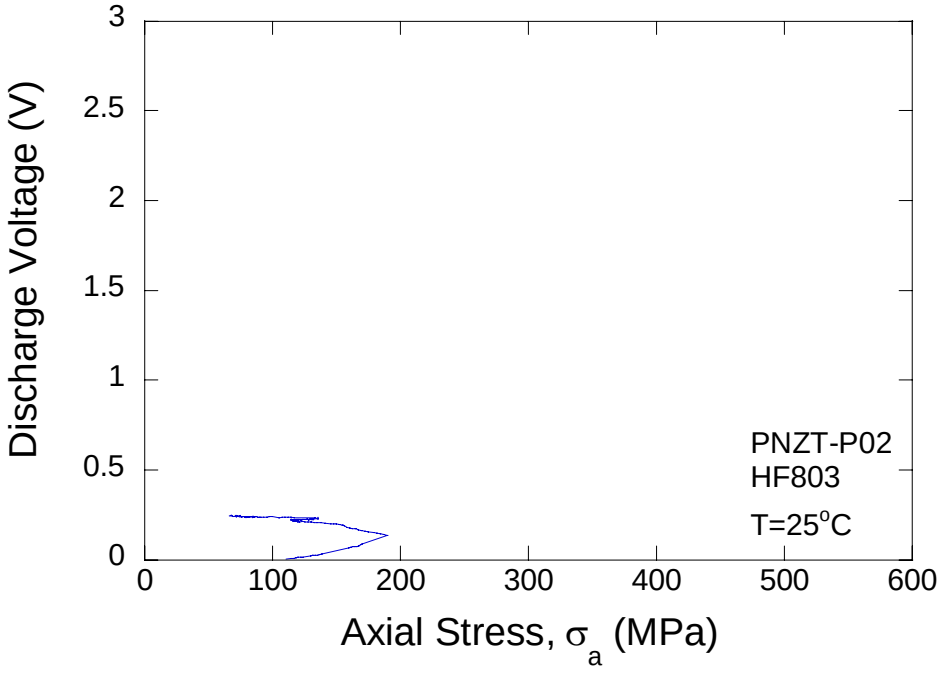
Discharge Voltage (V)
PNZT-P02
HF803
T=25°C
Axial Stress, σa (MPa)
3
2.5
2
1.5
1
0.5
0
0
100
200
300
400
500
600

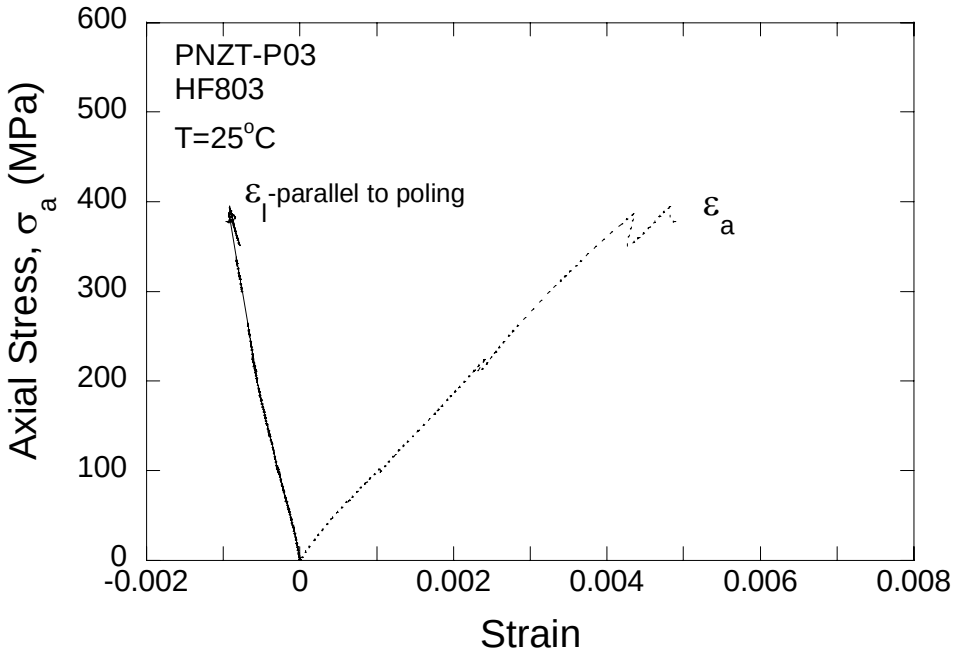
PNZT-P03
HF803
T=25°C
ε_l-parallel to poling
ε_a
Axial Stress, σ_a (MPa)
Strain
600
500
400
300
200
100
0
-0.002
0
0.002
0.004
0.006
0.008

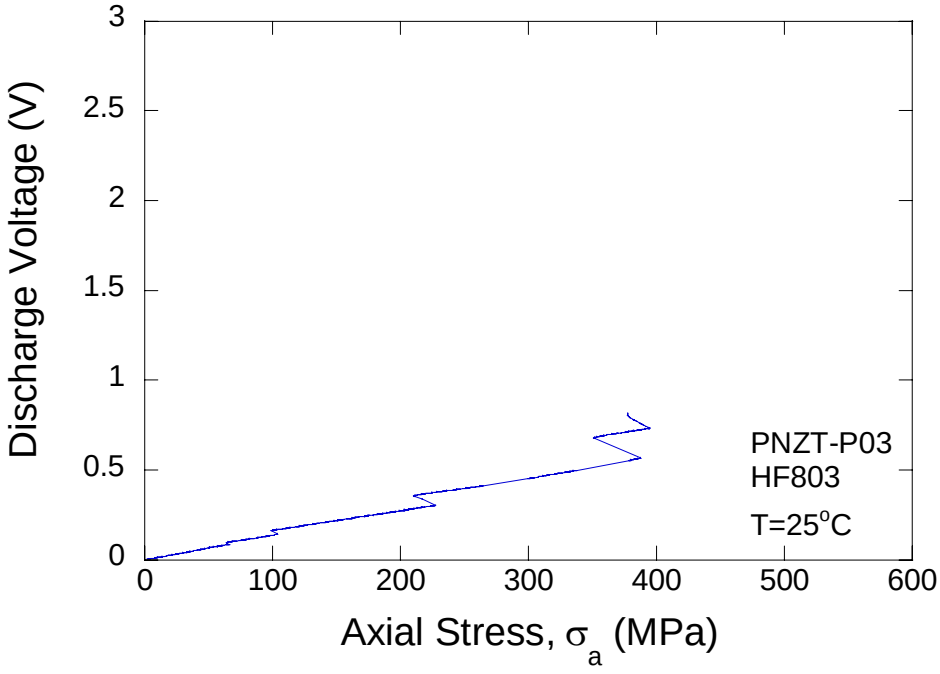
PNZT-P03
HF803
T=25°C
Discharge Voltage (V)
Axial Stress, σ_a (MPa)
3
2.5
2
1.5
1
0.5
0
0
100
200
300
400
500
600

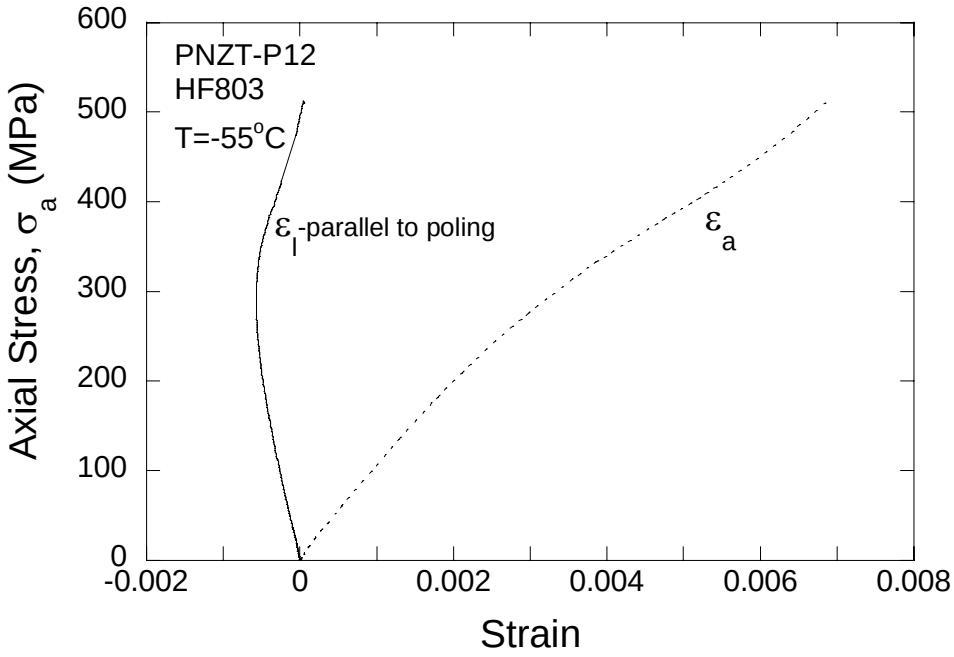
PNZT-P12
HF803
T=-55°C
ε_l-parallel to poling
ε_a
Axial Stress, σ_a (MPa)
Strain
600
500
400
300
200
100
0
-0.002
0
0.002
0.004
0.006
0.008

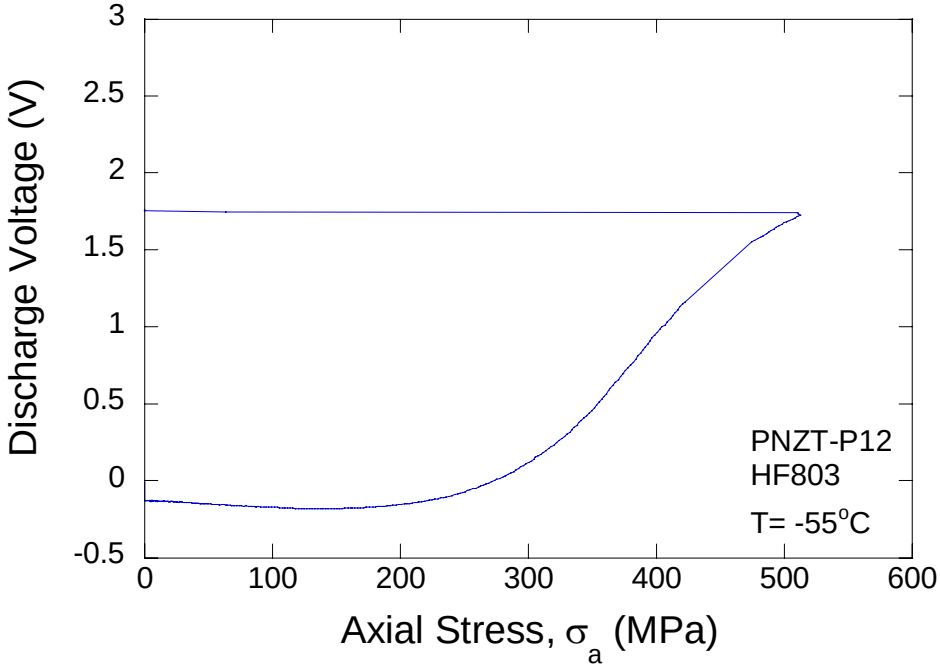
PNZT-P12
HF803
T= -55°C
Discharge Voltage (V)
Axial Stress, σ_a (MPa)
3
2.5
2
1.5
1
0.5
0
-0.5
0
100
200
300
400
500
600

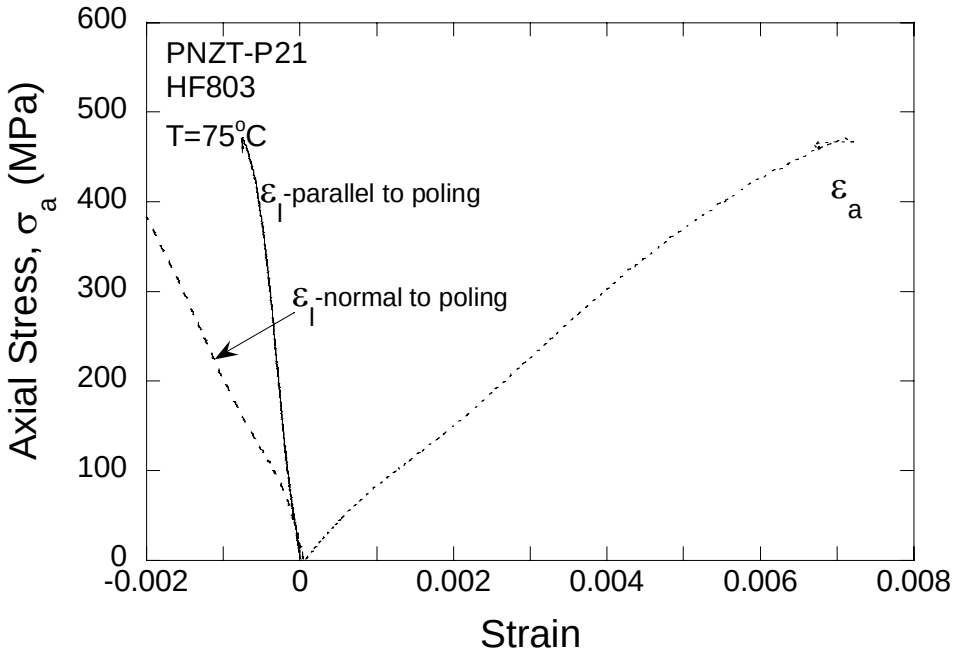
PNZT-P21
HF803
T=75°C
ε_l-parallel to poling
ε_l-normal to poling
ε_a
Axial Stress, σ_a (MPa)
Strain
600
500
400
300
200
100
0
-0.002
0
0.002
0.004
0.006
0.008

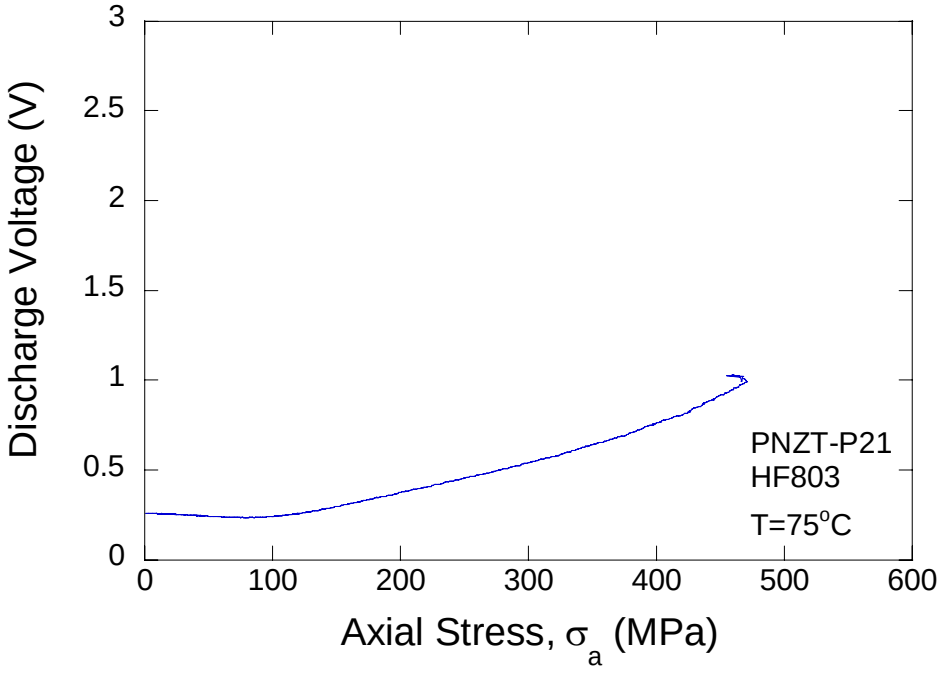
Discharge Voltage (V)
Axial Stress, σ_a (MPa)
PNZT-P21
HF803
T=75°C
3
2.5
2
1.5
1
0.5
0
0
100
200
300
400
500
600

APPENDIX C

Stress Paths, Discharged Voltages During Phase Transformation, and Stress-Strain Test Plots for Constant Stress Difference (CSD) Test for Poled PNZT-HF803 (σ_1- major principal stress acting in the long axis of the specimen, σ_3- confining pressure acting as the minor principal stress, ε_a-axial strain, $\varepsilon_{l\text{-parallel to poling}}$-lateral strain parallel to poling direction, and T-temperature)

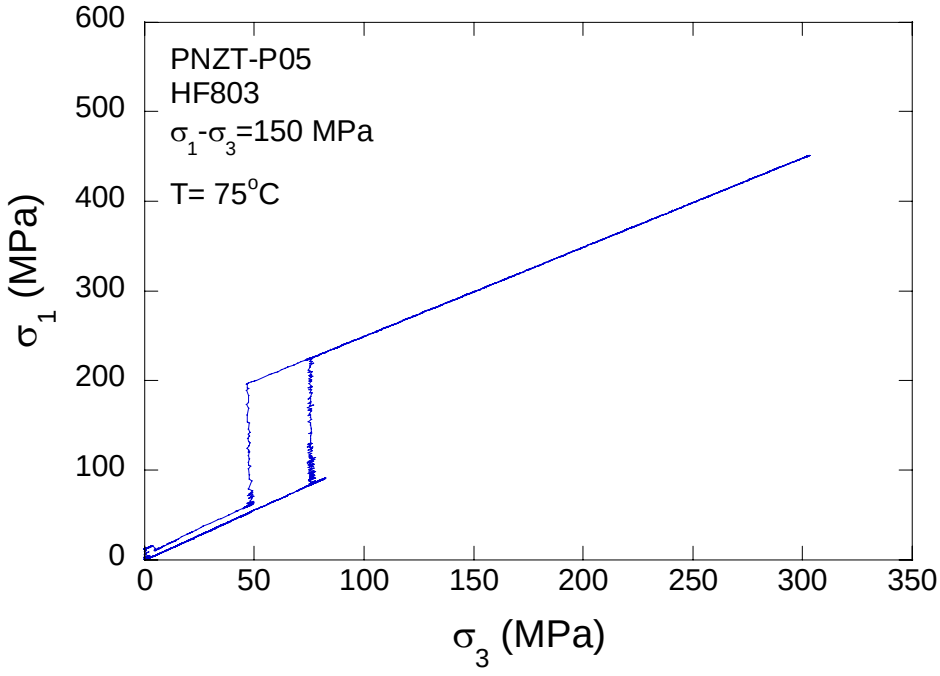
PNZT-P05
HF803
σ1-σ3=150 MPa
T= 75°C
σ1 (MPa)
σ3 (MPa)
0
100
200
300
400
500
600
0
50
100
150
200
250
300
350

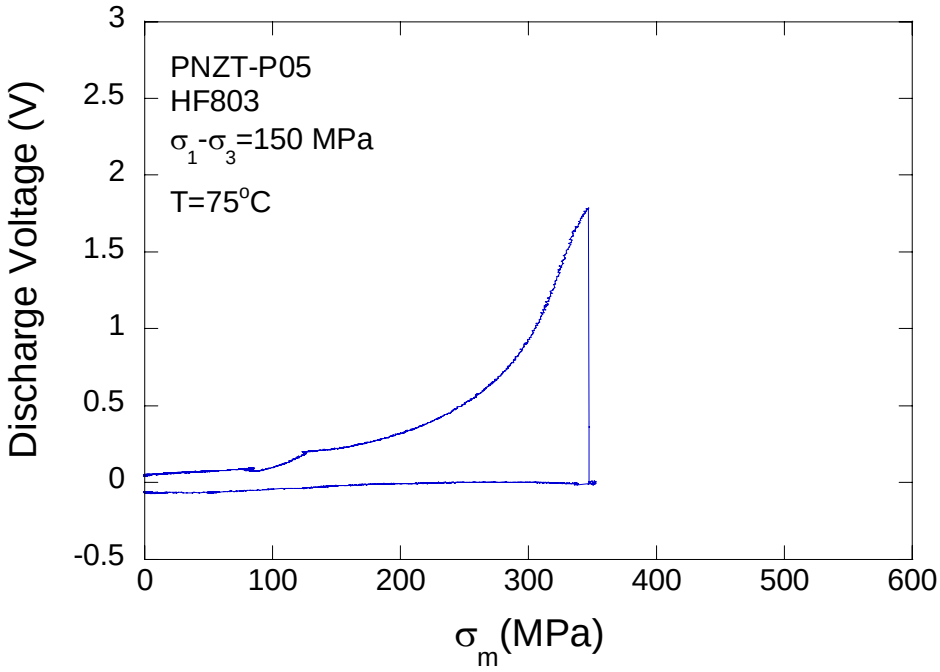
PNZT-P05
HF803
σ1-σ3=150 MPa
T=75°C
Discharge Voltage (V)
σm (MPa)
-0.5
0
0.5
1
1.5
2
2.5
3
0
100
200
300
400
500
600

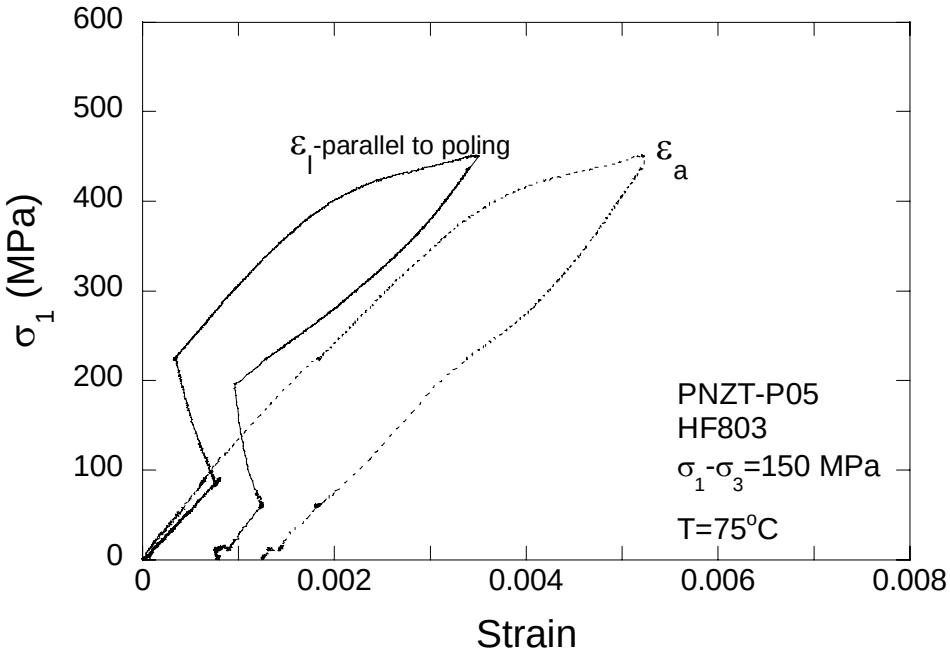
600
500
400
300
200
100
0
σ1 (MPa)
εl-parallel to poling
εa
PNZT-P05
HF803
σ1-σ3=150 MPa
T=75°C
0
0.002
0.004
0.006
0.008
Strain

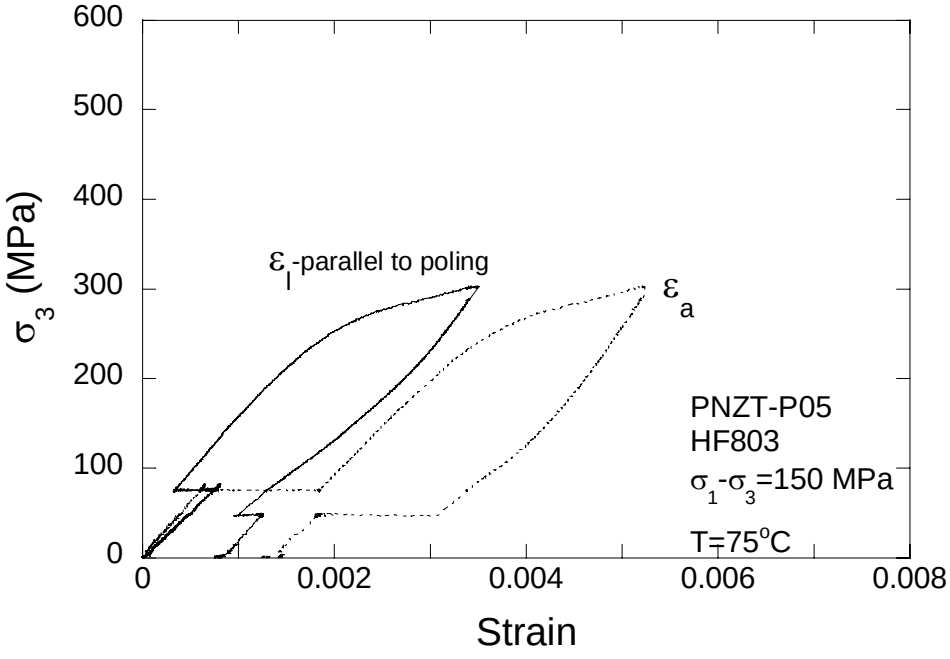
600
500
400
300
200
100
0
σ3 (MPa)
εl-parallel to poling
εa
PNZT-P05
HF803
σ1-σ3=150 MPa
T=75°C
0
0.002
0.004
0.006
0.008
Strain

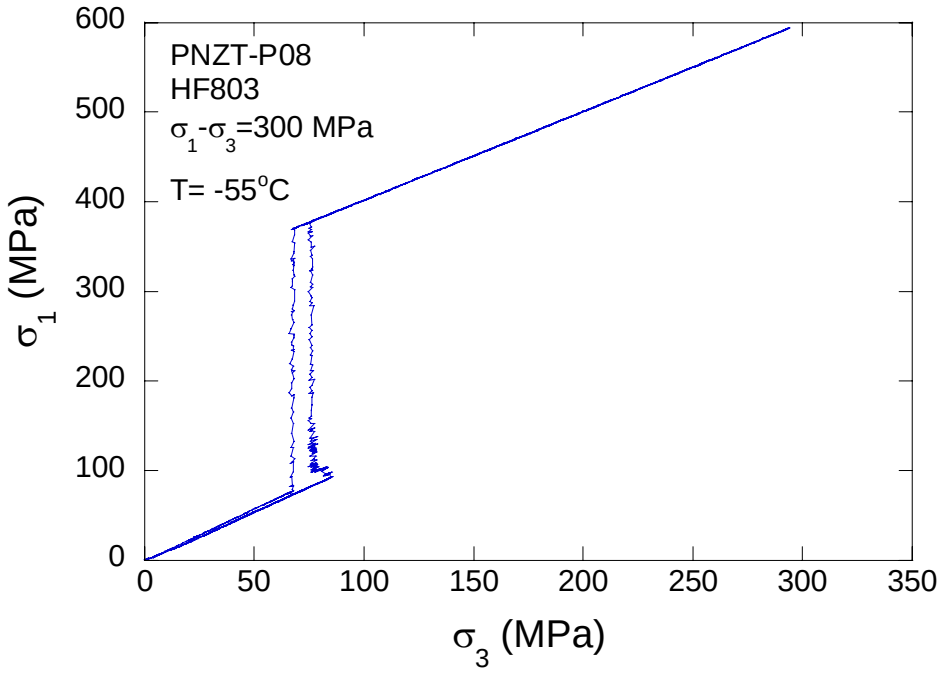
PNZT-P08
HF803
σ1-σ3=300 MPa
T= -55°C
σ1 (MPa)
σ3 (MPa)
0
100
200
300
400
500
600
0
50
100
150
200
250
300
350

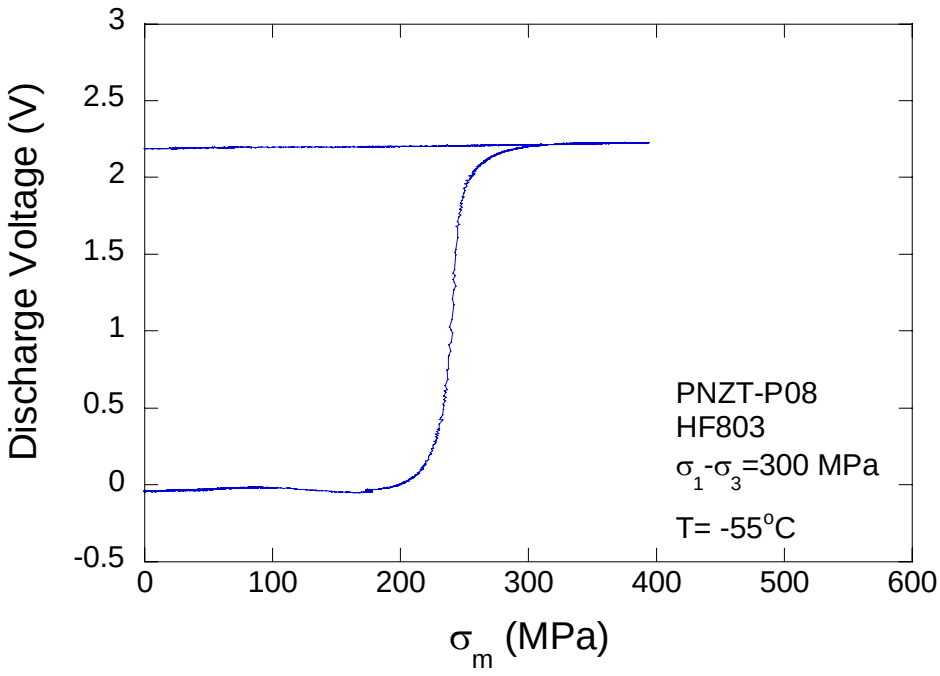
Discharge Voltage (V)
σm (MPa)
PNZT-P08
HF803
σ1-σ3=300 MPa
T= -55°C
-0.5
0
0.5
1
1.5
2
2.5
3
0
100
200
300
400
500
600

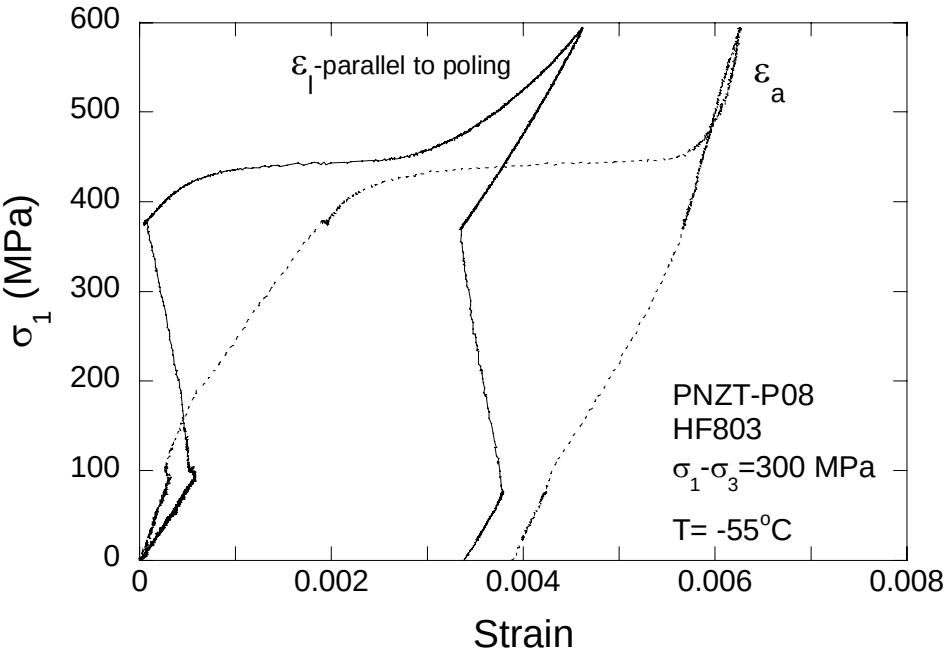
600
500
400
300
200
100
0
σ1 (MPa)
0
0.002
0.004
0.006
0.008
Strain
εl-parallel to poling
εa
PNZT-P08
HF803
σ1-σ3=300 MPa
T= -55°C

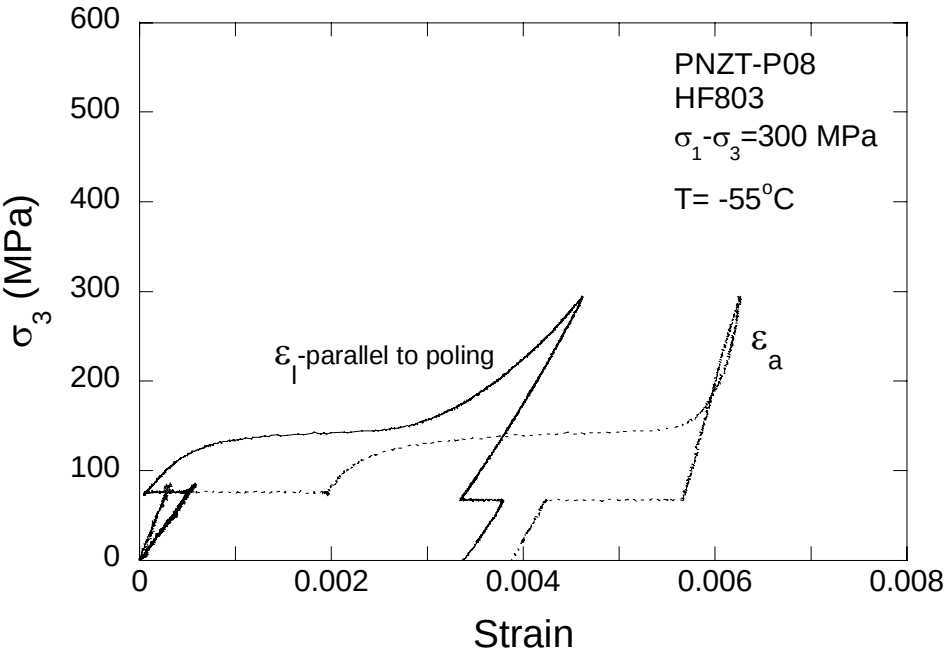
600
500
400
300
200
100
0
σ3 (MPa)
0
0.002
0.004
0.006
0.008
Strain
εl-parallel to poling
εa
PNZT-P08
HF803
σ1-σ3=300 MPa
T= -55°C

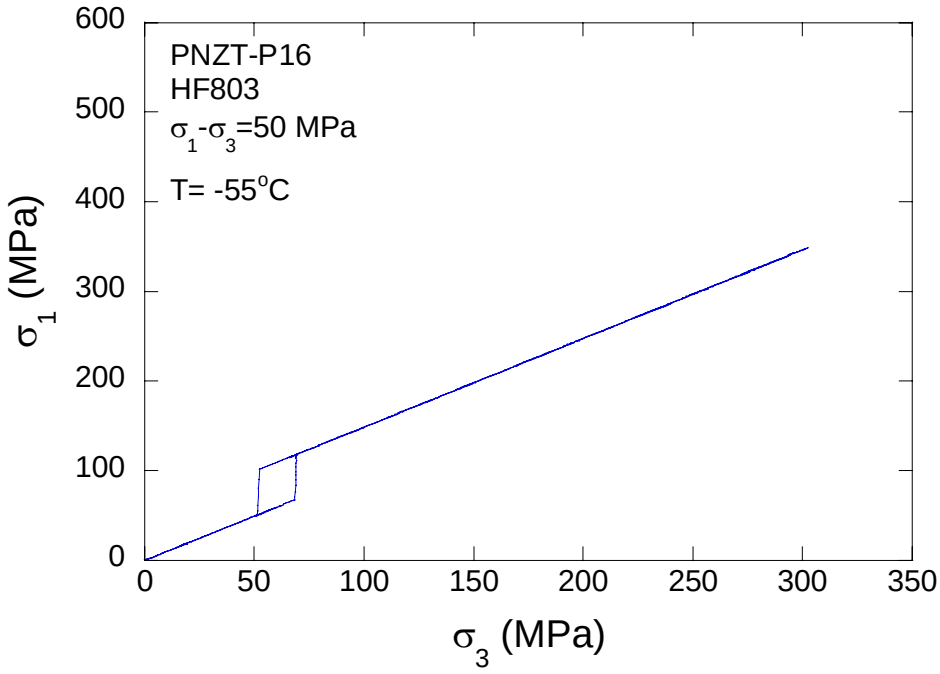
PNZT-P16
HF803
σ1-σ3=50 MPa
T= -55°C
σ1 (MPa)
σ3 (MPa)
0
100
200
300
400
500
600
0
50
100
150
200
250
300
350

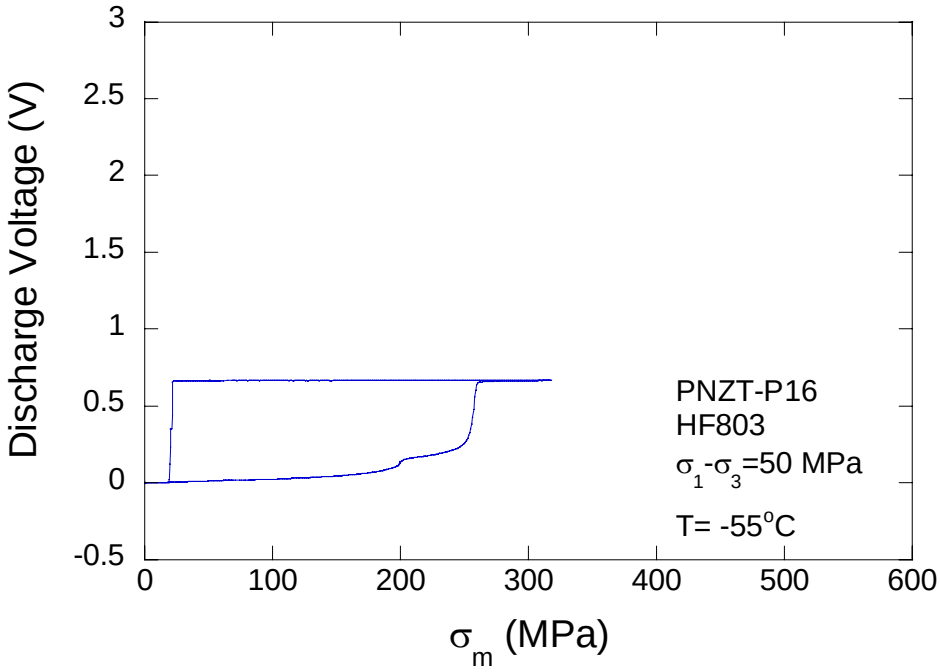
PNZT-P16
HF803
σ1-σ3=50 MPa
T= -55°C
Discharge Voltage (V)
σm (MPa)
-0.5
0
0.5
1
1.5
2
2.5
3
0
100
200
300
400
500
600

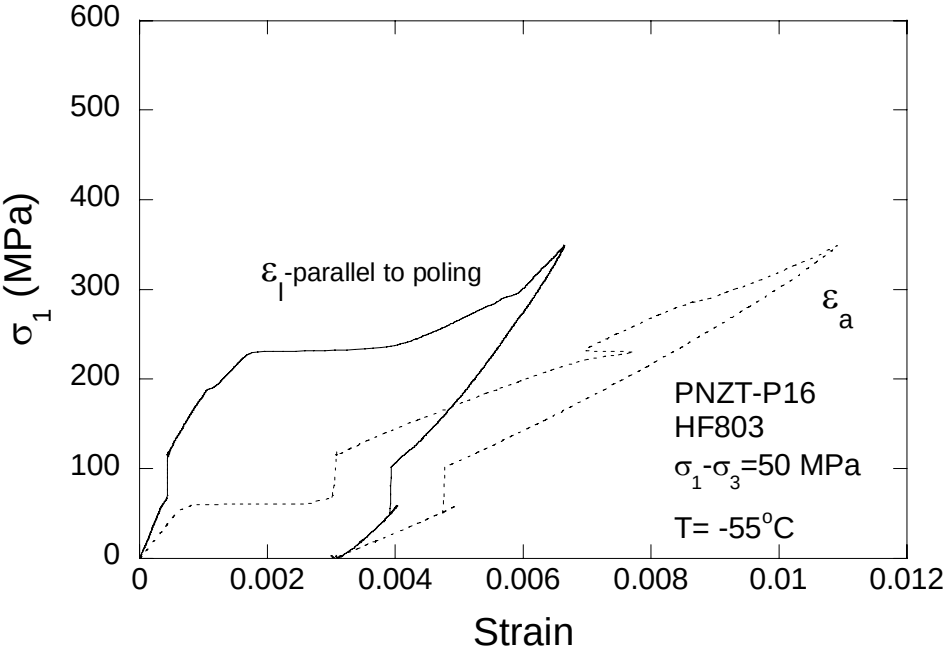
600
500
400
300
200
100
0
σ1 (MPa)
εl-parallel to poling
εa
PNZT-P16
HF803
σ1-σ3=50 MPa
T= -55°C
0
0.002
0.004
0.006
0.008
0.01
0.012
Strain

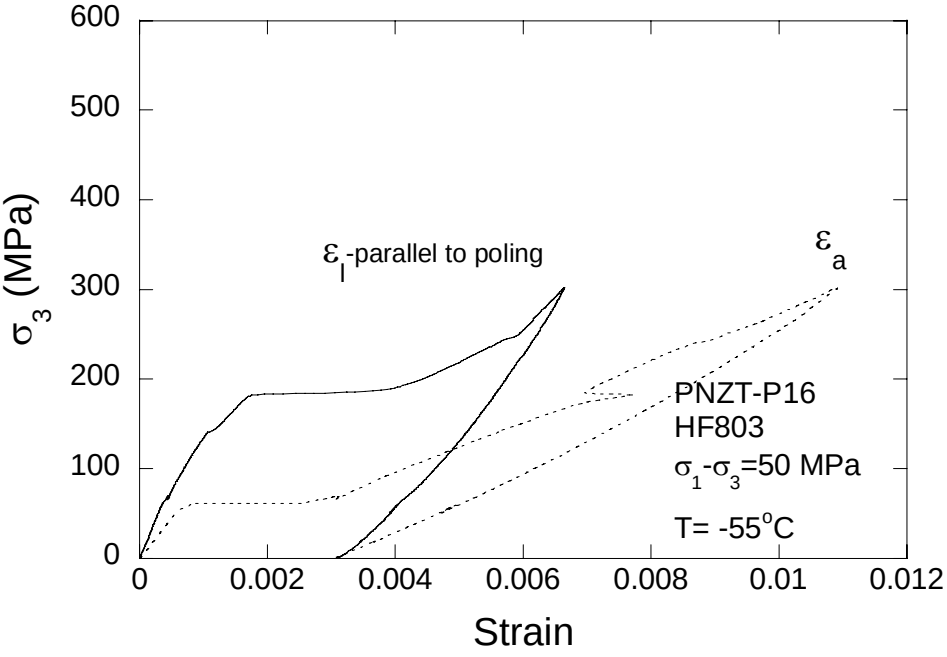
600
500
400
300
200
100
0
σ3 (MPa)
εl-parallel to poling
εa
PNZT-P16
HF803
σ1-σ3=50 MPa
T= -55°C
0
0.002
0.004
0.006
0.008
0.01
0.012
Strain

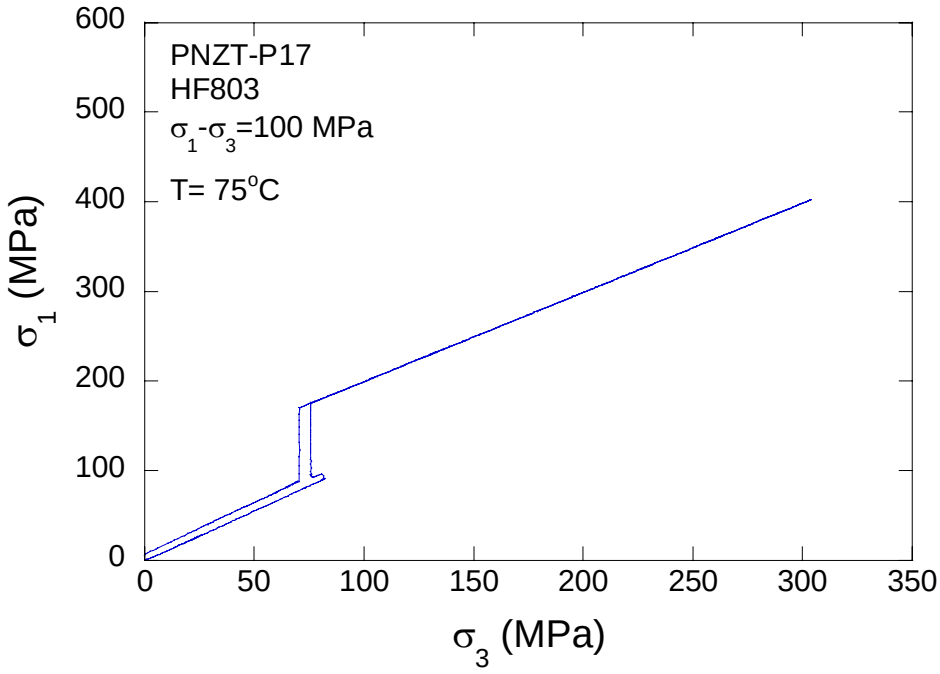
PNZT-P17
HF803
σ1-σ3=100 MPa
T= 75°C
σ1 (MPa)
σ3 (MPa)
0
100
200
300
400
500
600
0
50
100
150
200
250
300
350

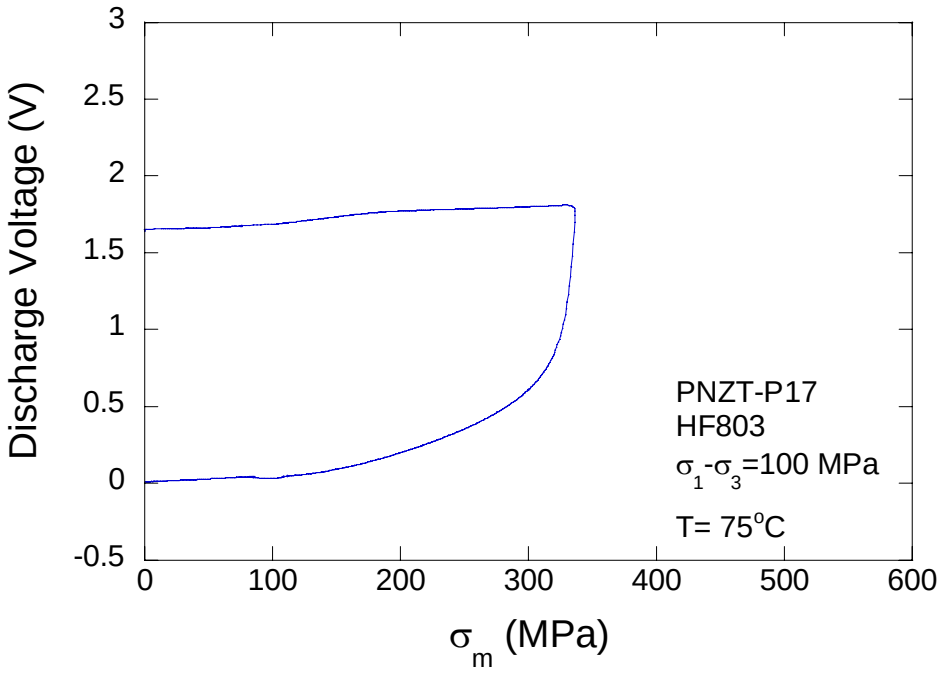
PNZT-P17
HF803
σ1-σ3=100 MPa
T= 75°C
Discharge Voltage (V)
σm (MPa)
-0.5
0
0.5
1
1.5
2
2.5
3
0
100
200
300
400
500
600

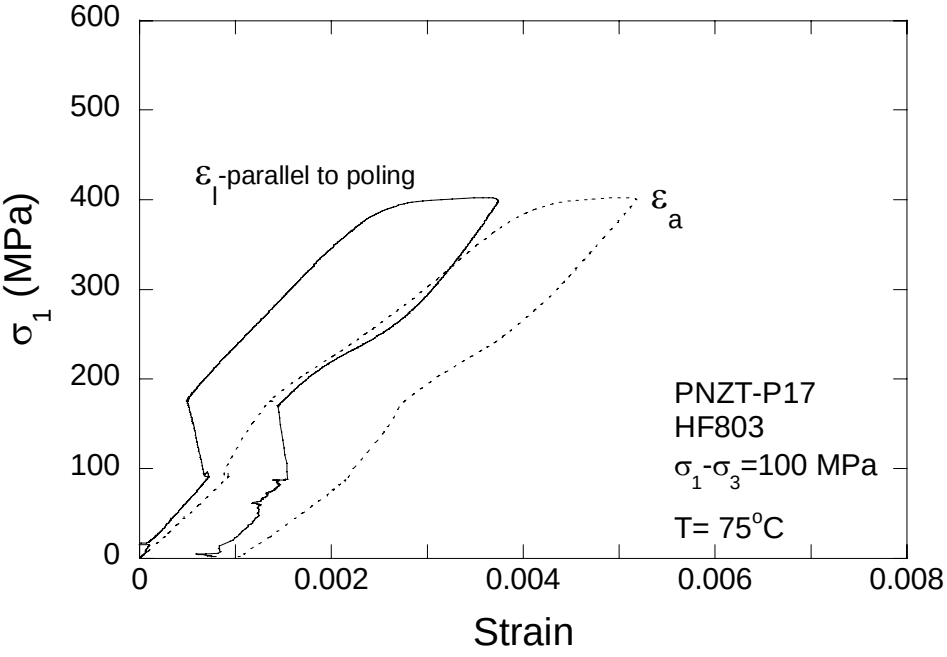
600
500
400
300
200
100
0
σ1 (MPa)
εl-parallel to poling
εa
PNZT-P17
HF803
σ1-σ3=100 MPa
T= 75°C
0
0.002
0.004
0.006
0.008
Strain

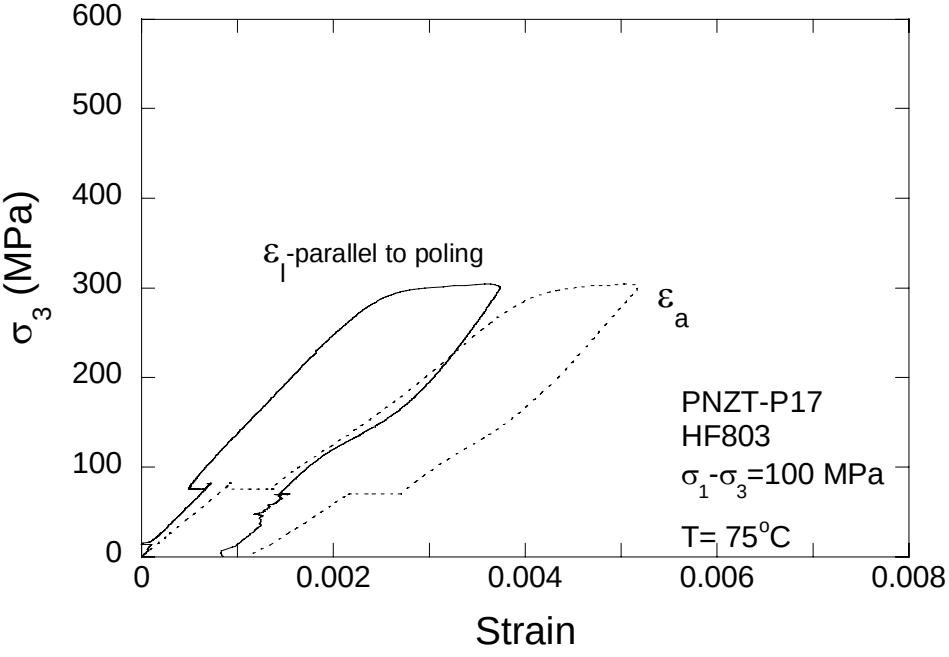
600
500
400
300
200
100
0
σ3 (MPa)
εl-parallel to poling
εa
PNZT-P17
HF803
σ1-σ3=100 MPa
T= 75°C
0
0.002
0.004
0.006
0.008
Strain

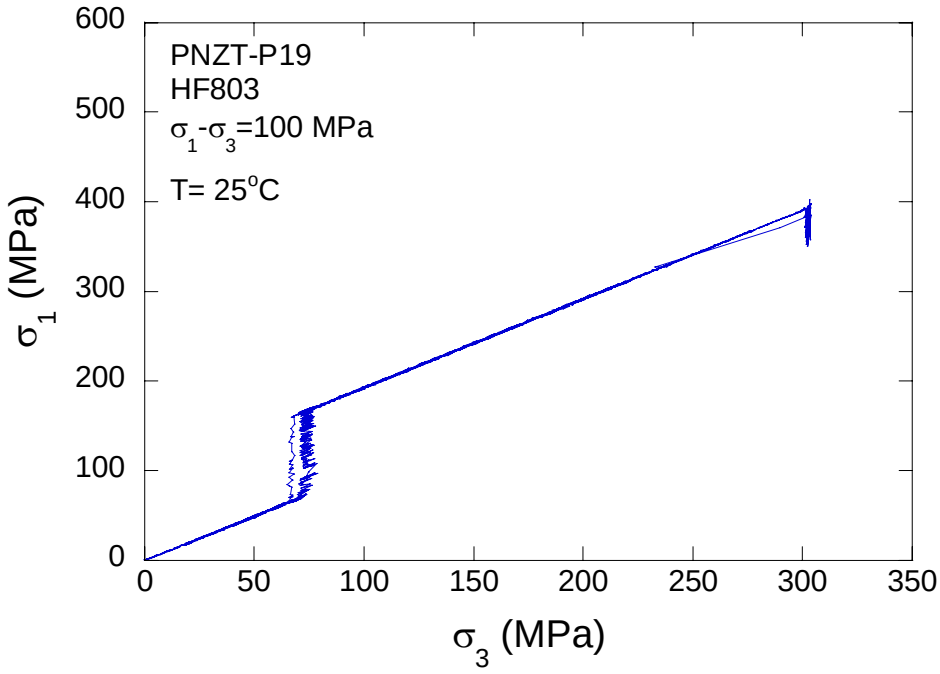
PNZT-P19
HF803
σ1-σ3=100 MPa
T= 25°C
σ1 (MPa)
σ3 (MPa)
0
100
200
300
400
500
600
0
50
100
150
200
250
300
350

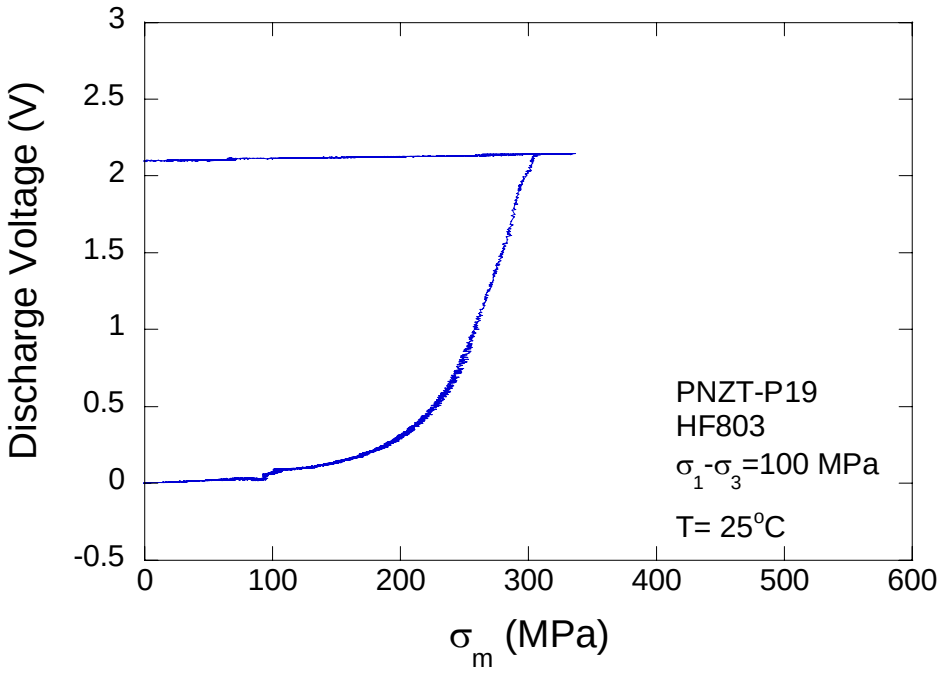
PNZT-P19
HF803
σ1-σ3=100 MPa
T= 25°C
Discharge Voltage (V)
σm (MPa)
-0.5
0
0.5
1
1.5
2
2.5
3
0
100
200
300
400
500
600

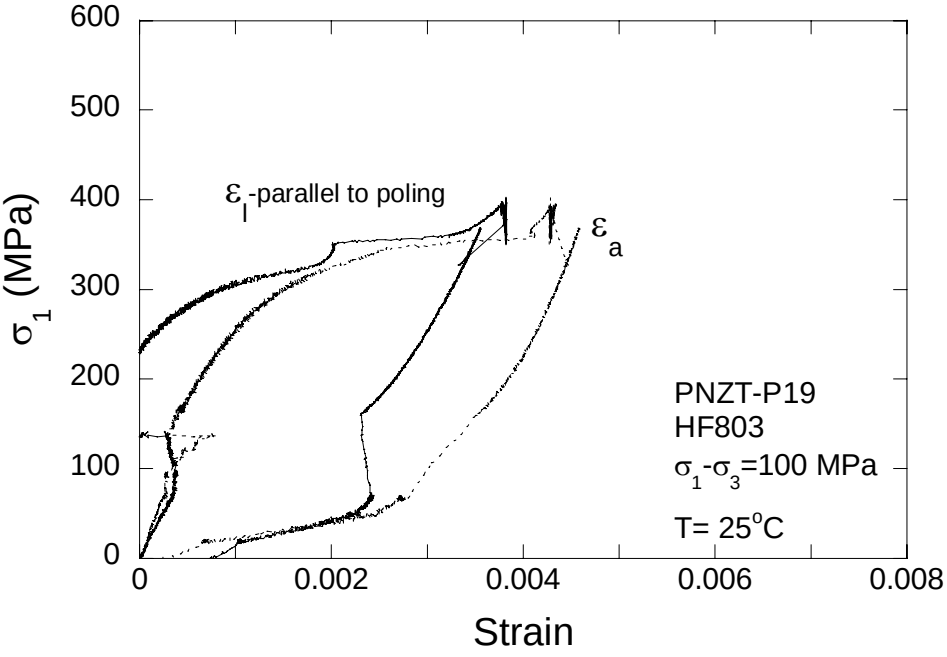
600
500
400
300
200
100
0
σ1 (MPa)
εl-parallel to poling
εa
PNZT-P19
HF803
σ1-σ3=100 MPa
T= 25°C
0
0.002
0.004
0.006
0.008
Strain

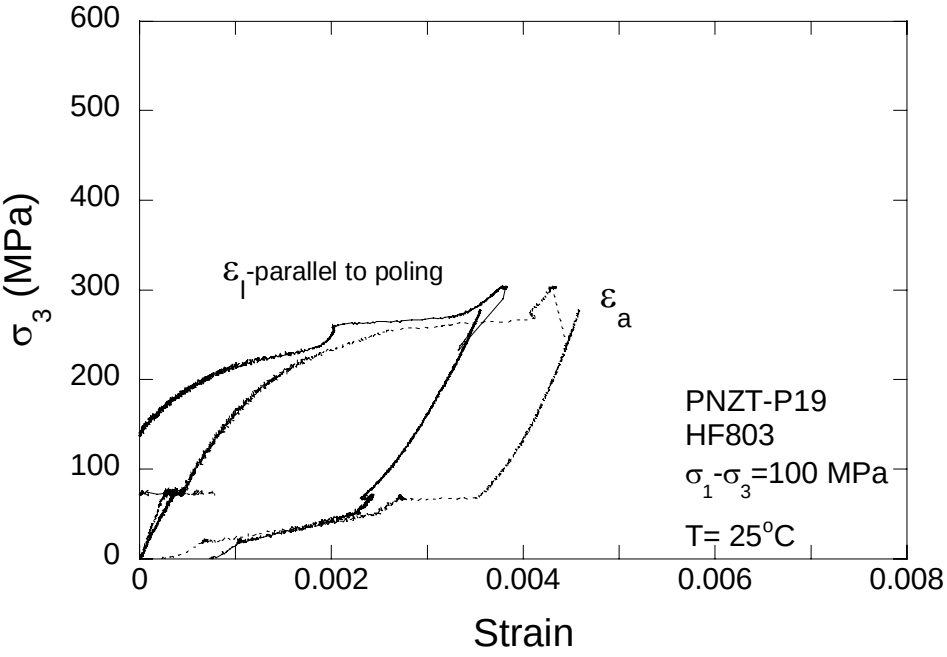
600
500
400
300
200
100
0
σ3 (MPa)
εl-parallel to poling
εa
PNZT-P19
HF803
σ1-σ3=100 MPa
T= 25°C
0
0.002
0.004
0.006
0.008
Strain

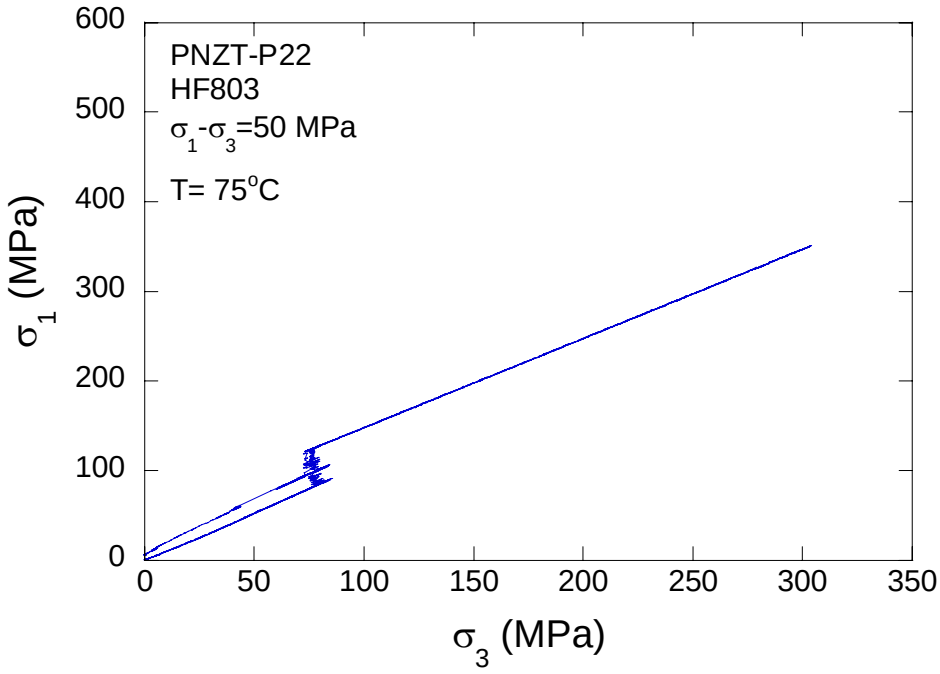
PNZT-P22
HF803
σ1-σ3=50 MPa
T= 75°C
σ1 (MPa)
σ3 (MPa)
0
100
200
300
400
500
600
0
50
100
150
200
250
300
350

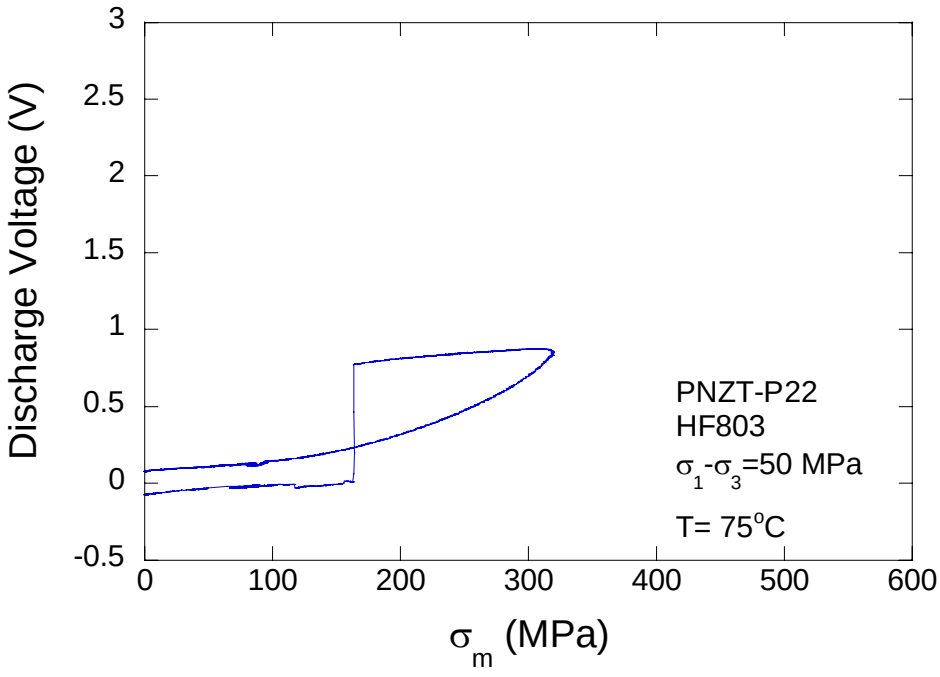
PNZT-P22
HF803
σ1-σ3=50 MPa
T= 75°C
Discharge Voltage (V)
σm (MPa)
3
2.5
2
1.5
1
0.5
0
-0.5
0
100
200
300
400
500
600

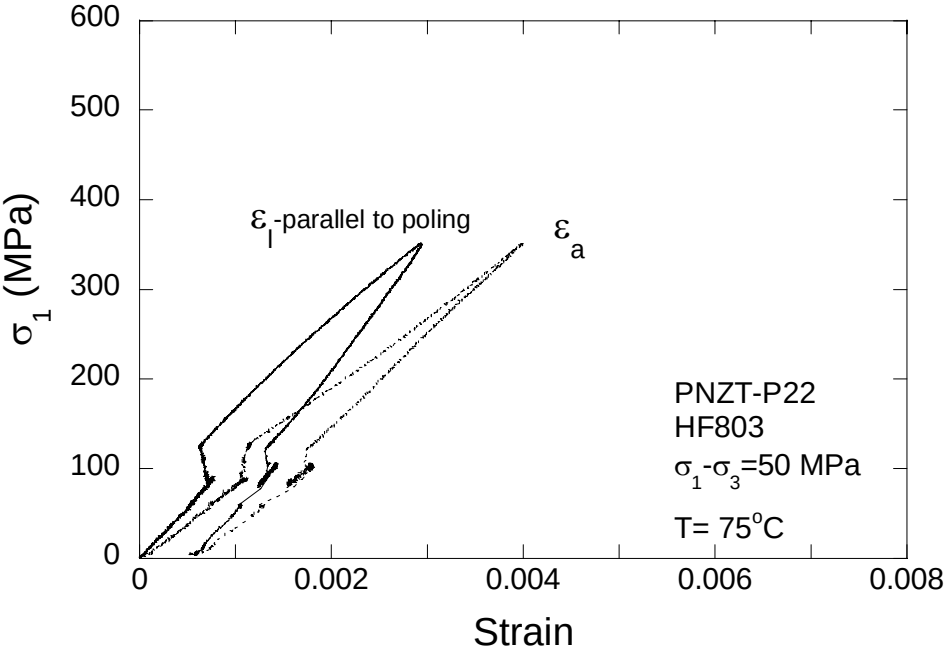
600
500
400
300
200
100
0
σ1 (MPa)
εl-parallel to poling
εa
PNZT-P22
HF803
σ1-σ3=50 MPa
T= 75°C
0
0.002
0.004
0.006
0.008
Strain

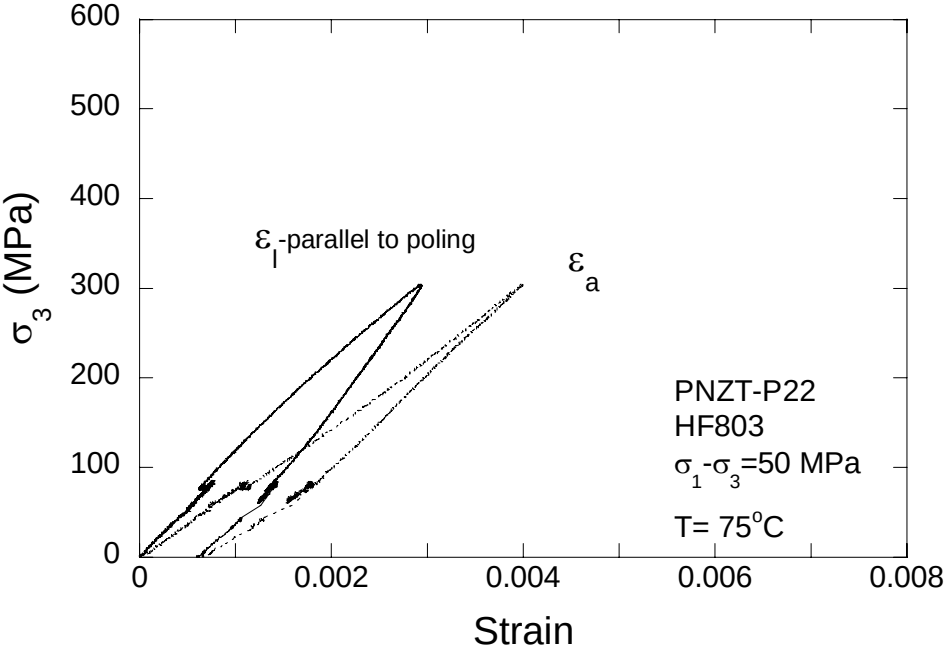
600
500
400
300
200
100
0
σ3 (MPa)
εl-parallel to poling
εa
PNZT-P22
HF803
σ1-σ3=50 MPa
T= 75°C
0
0.002
0.004
0.006
0.008
Strain

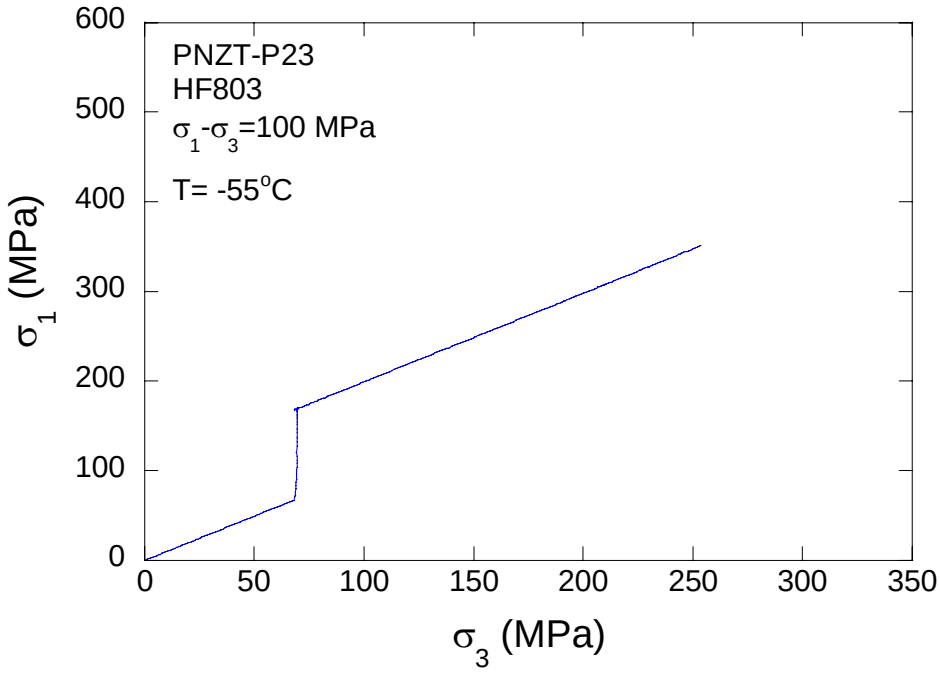
PNZT-P23
HF803
σ1-σ3=100 MPa
T= -55°C
σ1 (MPa)
σ3 (MPa)
0
100
200
300
400
500
600
0
50
100
150
200
250
300
350

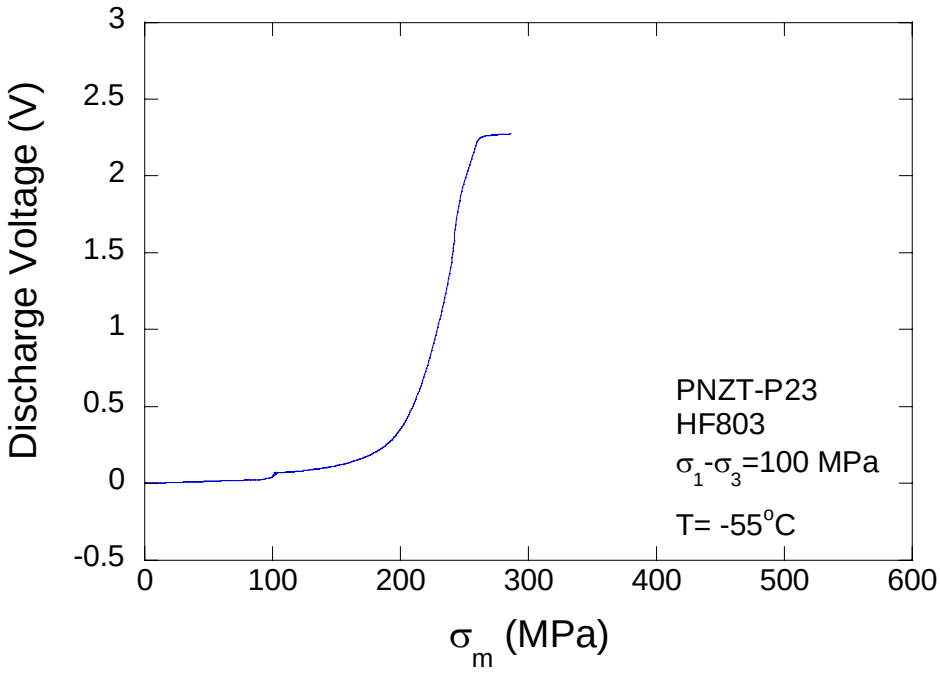
PNZT-P23
HF803
σ1-σ3=100 MPa
T= -55°C
Discharge Voltage (V)
σm (MPa)
-0.5
0
0.5
1
1.5
2
2.5
3
0
100
200
300
400
500
600

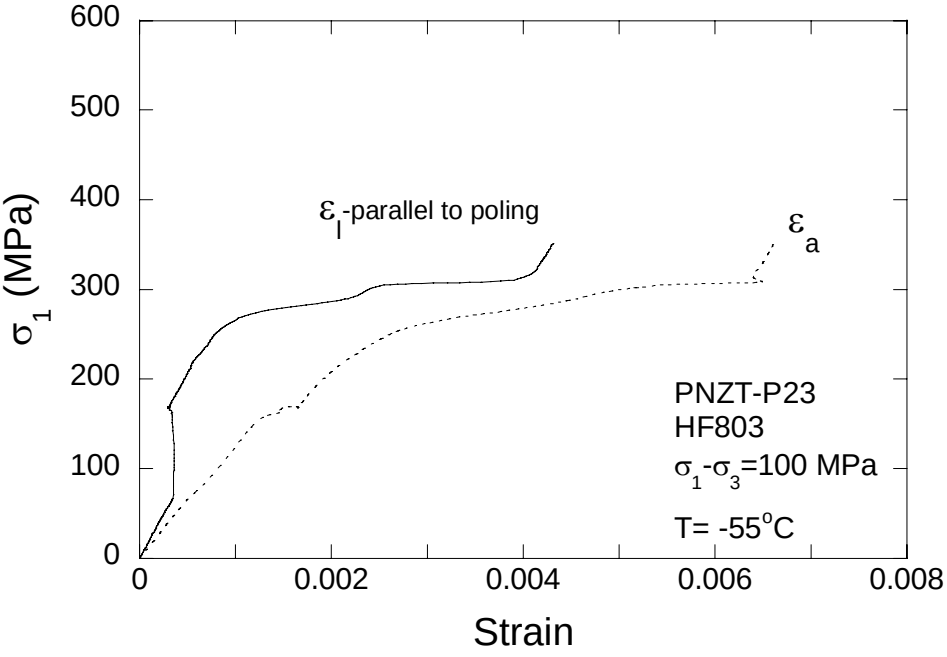
600
500
400
300
200
100
0
σ1 (MPa)
εl-parallel to poling
εa
PNZT-P23
HF803
σ1-σ3=100 MPa
T= -55°C
0
0.002
0.004
0.006
0.008
Strain

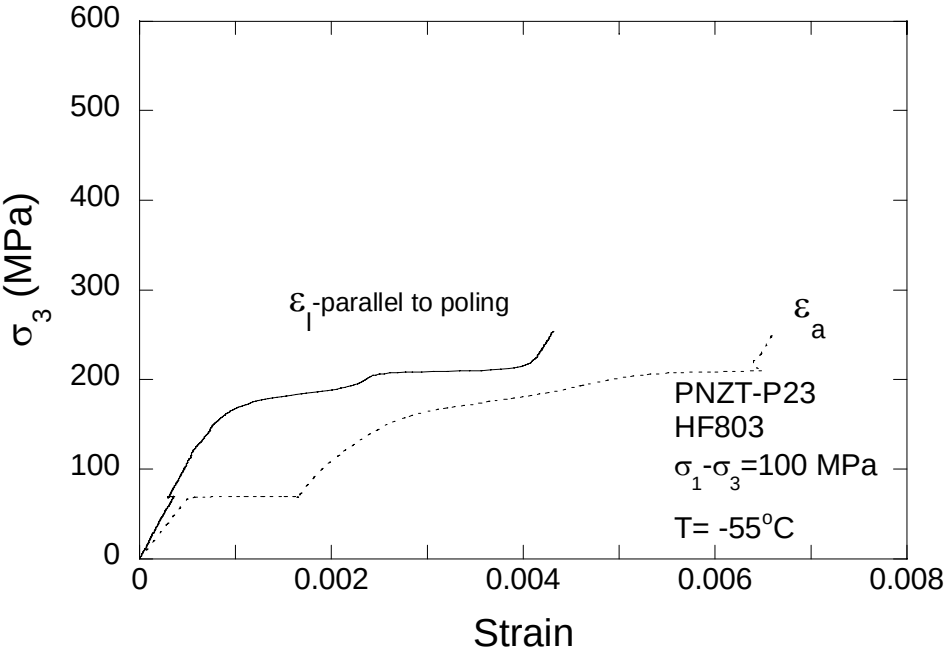
600
500
400
300
200
100
0
σ3 (MPa)
εl-parallel to poling
εa
PNZT-P23
HF803
σ1-σ3=100 MPa
T= -55°C
0
0.002
0.004
0.006
0.008
Strain

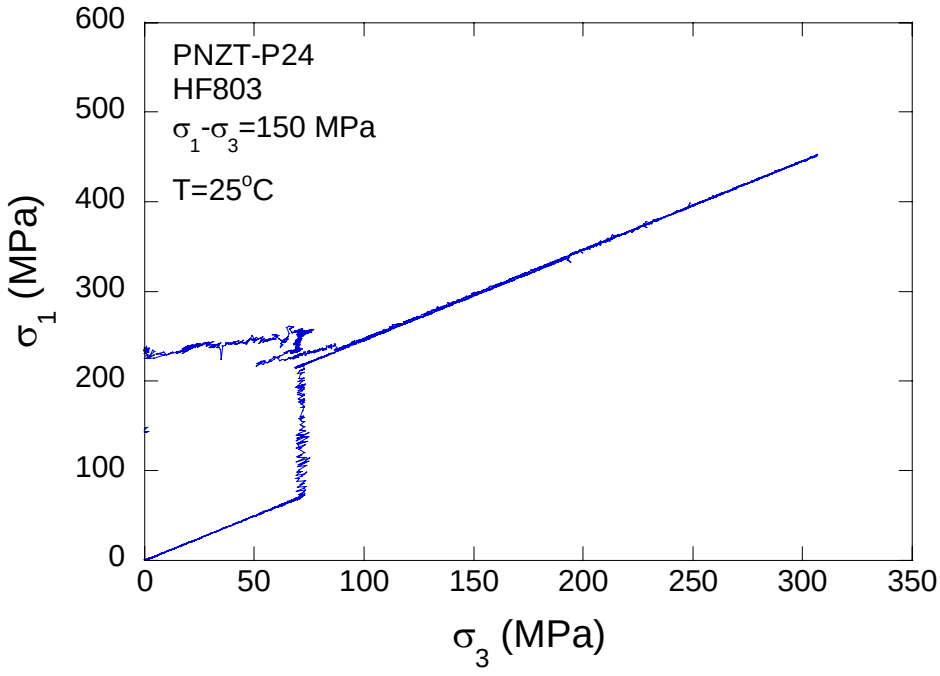
PNZT-P24
HF803
σ1-σ3=150 MPa
T=25°C
σ1 (MPa)
σ3 (MPa)
0
100
200
300
400
500
600
0
50
100
150
200
250
300
350

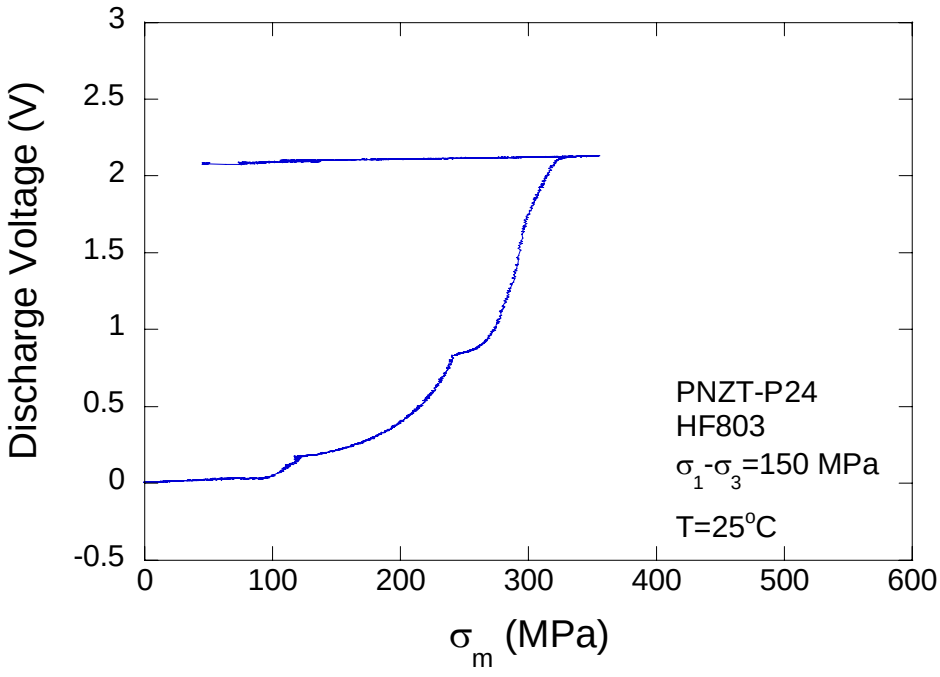
PNZT-P24
HF803
σ1-σ3=150 MPa
T=25°C
Discharge Voltage (V)
σm (MPa)
-0.5
0
0.5
1
1.5
2
2.5
3
0
100
200
300
400
500
600

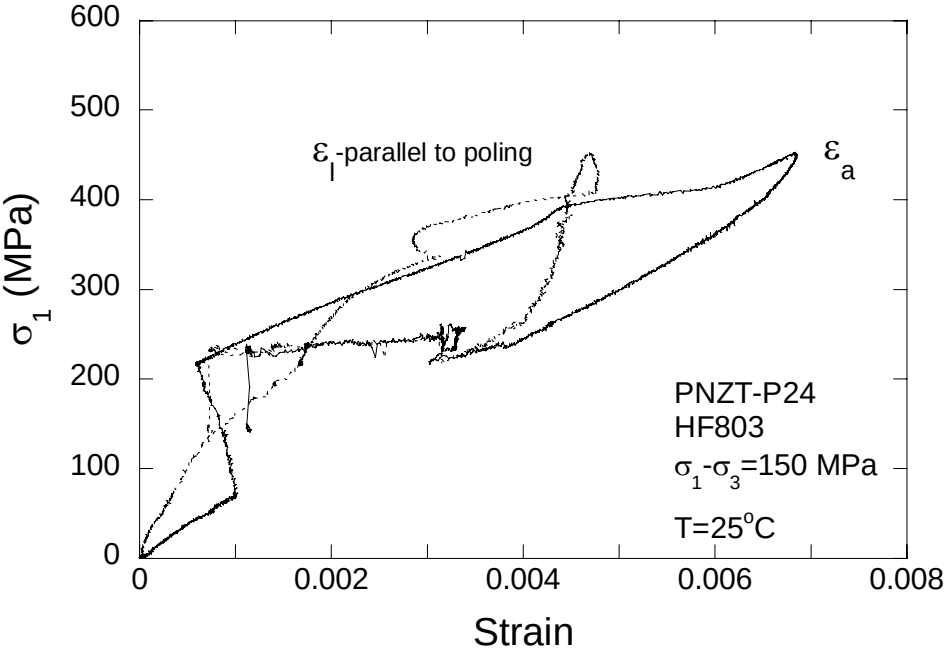
600
500
400
300
200
100
0
σ1 (MPa)
εl-parallel to poling
εa
PNZT-P24
HF803
σ1-σ3=150 MPa
T=25°C
0
0.002
0.004
0.006
0.008
Strain

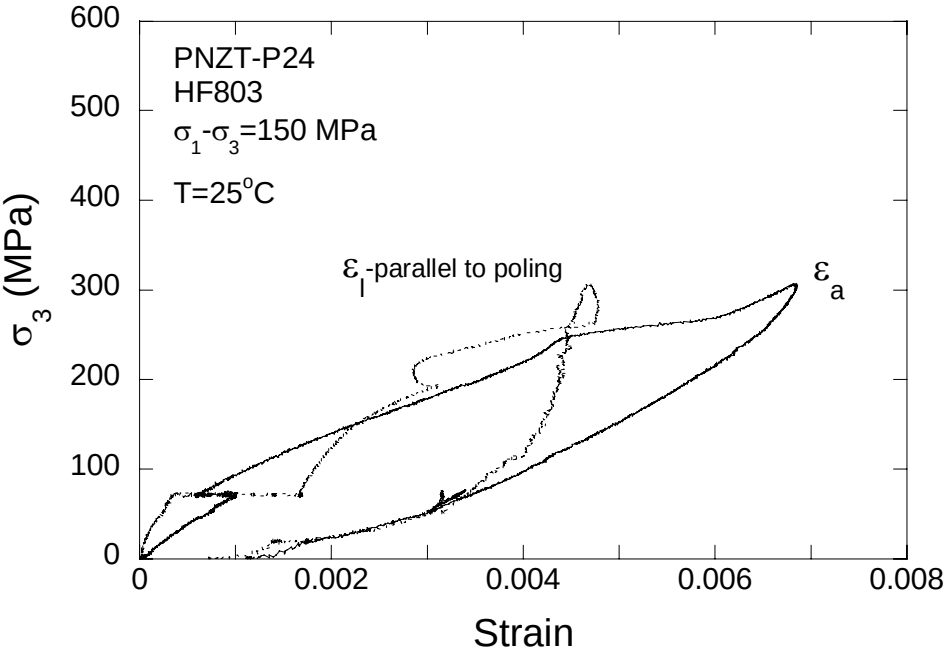
600
500
400
300
200
100
0
σ3 (MPa)
PNZT-P24
HF803
σ1-σ3=150 MPa
T=25°C
εl-parallel to poling
εa
0
0.002
0.004
0.006
0.008
Strain

APPENDIX D

List of Data and Supplemental Files Archived in Webfileshare System for Poled PNZT-HF803

List of files archived in the WEBFILESHARE system (https://wfsprod01.sandia.gov).

Folder Name	File Name	Description
/TARGET/PNZT-803	PNZT-SAND04.doc	This SAND report: SAND2004-4954
/TARGET/PNZT-803	PNZT-HF803-Poled-master.xls	Master data file consists of the following four worksheets: **Specimen**: PNZT specimen dimensions and test matrix **Hydrostatic Compression**: Hydrostatic Compression test data for PNZT-P11, P07, P-09, and P-01 consisting of time, pressure, axial stress, lateral strain in poling direction, estimated volumetric strain, corrected volumetric strain, and discharge voltage. **Uniaxial Compression**: Uniaxial compression test data for PNZT-P12, P18, P02, P03 and P21 consisting of time, pressure (=0), axial stress, lateral strain in poling direction, and discharge voltage. **CSD**: Constant Stress Difference test data for PNZT-P11, P16, P23, and P08 (-55°C); PNZT-P07, P19, and P24 (25°C); and PNZT-P01, P22, P17, and P05 (75°C). The data consist of time, pressure, axial stress, lateral strain in poling direction, estimated volumetric strain, corrected volumetric strain and discharge voltage.
/TARGET/PNZT-803	Poled 803-data sheet.zip	Laboratory data sheets for the following tests: PNZT-P01, P02, P03, P05, P07, P08, P09, P11, P12, P13, P14, P15, P16, P17, P18, P19, P21, P22, P23, and P24

DISTRIBUTION

Sandia National Laboratories
P.O. Box 5800
Albuquerque, NM 87185

1	MS 0512	T. E. Blejwas, 2500
1	MS 0515	S. G. Barnhart, 2561
1	MS 0515	T. A. Haverlock, 2561
1	MS 0515	J. D. Keck, 2561
1	MS 0515	D. K. Morgan, 2561
1	MS 0515	R. A. Pike, 2561
1	MS 0515	T. W. Scofield, 2561
1	MS 0515	B. J. Wells, 2561
1	MS 0516	B. H. Cole, 2564
1	MS 0516	S. C. Hwang, 2564
1	MS 0516	R. G. Spulak, 2564
1	MS 0521	C. L. Knapp, 2560
1	MS 0521	R. A. Damerow, 2561
5	MS 0521	S. T. Montgomery, 2561
1	MS 0701	P. J. Davies, 6100
1	MS 0751	R. M. Brannon, 6117
1	MS 0751	L. S. Costin, 6117
1	MS 0751	D. J. Holcomb, 6117
5	MS 0751	M. Y. Lee, 6117
1	MS 0751	T. W. Pfeifle, 6117
1	MS 0819	J. Robbins, 9231
3	MS 0824	J. L. Moya, 9130
1	MS 0828	M. Pilch, 9133
1	MS 0834	J. E. Johannes, 9114
1	MS 0841	T. C. Bickel, 9100
1	MS 0889	J. S. Glass, 1843
1	MS 0889	C. S. Watson, 1843
1	MS 0959	S. J. Lockwood, 14192
1	MS 0959	R. H. Moore, 14192
1	MS 0959	P. Yang, 14192
2	MS 1031	J. H. Hofer, 6117
1	MS 1181	L. C. Chhabildas, 1647
1	MS 1181	M. D. Furnish, 1647
1	MS 1186	R. J. Lawrence, 1674
1	MS 1395	B. Y. Park, 6821
1	MS 1411	H. E. Fang, 1834
1	MS 1411	B. A. Tuttle, 1843
1	MS 1411	V. Tikare, 1834
1	MS 1421	M. U. Anderson, 1122
1	MS 1421	G. A. Samara, 1122
1	MS 1421	R. E. Setchell, 1122
1	MS 9018	Central Tech. Files, 8945-1

2	MS 0899	Technical Library, 9616
2	MS 0731	823/Library, 6850

P.O. Box 808
Livermore, CA 94551

Roger Logan, L-25

Los Alamos National Laboratory
P.O. Box 1663
Los Alamos, NM 87545

Bill Bearden MS F602
Steve Girrens, ESA-EA, P946
Dick Macek MS P946

Kevin C. Greenaugh
Department of Energy/Defense Programs
Director, Division of System Simulation & Validation
1000 Independence Ave., SW
Washington DC 20585

Bill-Roy Harrison
Department of Energy/Defense Programs
Program Manager, Weapons Systems Engineering Certification Campaign
19901 Germantown Rd
Germantown, MD 20874

Diane Bird
Weapons Assessments and Development
Supervisory General Engineer
1000 Independence Ave.
NA-115.1
Washington DC 20585